The Planetary Science Journal, 2:173 (24pp), 2021 October https://doi.org/10.3847/PSJ/ac063e

The Double Asteroid Redirection Test (DART): Planetary Defense Investigations and Requirements

Andrew S. Rivkin[1], Nancy L. Chabot[1], Angela M. Stickle[1], Cristina A. Thomas[2], Derek C. Richardson[3], Olivier Barnouin[1], Eugene G. Fahnestock[4], Carolyn M. Ernst[1], Andrew F. Cheng[1], Steven Chesley[4], Shantanu Naidu[4], Thomas S. Statler[5], Brent Barbee[6], Harrison Agrusa[3], Nicholas Moskovitz[7], R. Terik Daly[1], Petr Pravec[8], Petr Scheirich[8], Elisabetta Dotto[9], Vincenzo Della Corte[10], Patrick Michel[11], Michael Küppers[12], Justin Atchison[1], and Masatoshi Hirabayashi[13]

[1] Johns Hopkins University Applied Physics Laboratory, 11100 Johns Hopkins Road, Laurel, MD, 20723, USA; andy.rivkin@jhuapl.edu
[2] Northern Arizona University, Department of Astronomy and Planetary Science, P.O. Box 6010, Flagstaff, AZ 86011, USA
[3] Department of Astronomy, University of Maryland, College Park, MD 20742-2421, USA
[4] Jet Propulsion Laboratory, California Institute of Technology, 4800 Oak Grove Drive, Pasadena, CA 91109, USA
[5] NASA Headquarters, Washington, DC 20546, USA
[6] NASA Goddard Space Flight Center, 8800 Greenbelt Road, Greenbelt, MD 20771, USA
[7] Lowell Observatory, 1400 West Mars Hill Road, Flagstaff, AZ 86001, USA
[8] Astronomical Institute, Academy of Sciences of the Czech Republic, Fričova 1, Ondřejov CZ-25165, Czech Republic
[9] INAF Osservatorio Astronomico di Roma, Via Frascati 33, 00078, Monte Porzio Catone, Roma, Italy
[10] INAF Istituto di Astrofisica e Planetologia Spaziali, Via Fosso del Cavaliere 100, 00133, Roma, Italy
[11] Université Côte d'Azur, Observatoire de la Côte d'Azur, CNRS, Lagrange Laboratory, France
[12] European Space Astronomy Centre, European Space Agency, Urbanización Villafranca del Castillo, Villanueva de la Cañada, E-28692 Madrid, Spain
[13] Aerospace Engineering, Auburn University, Auburn, AL, 36849, USA
Received 2021 January 6; revised 2021 May 21; accepted 2021 May 21; published 2021 August 25

Abstract

The Double Asteroid Redirection Test (DART) is a Planetary Defense mission, designed to demonstrate the kinetic impactor technique on (65803) Didymos I Dimorphos, the secondary of the (65803) Didymos system. DART has four level 1 requirements to meet in order to declare mission success: (1) impact Dimorphos between 2022 September 25 and October 2, (2) cause at least a 73 s change in its binary orbit period via the impact, (3) measure the change in binary period to an uncertainty of 7.3 s or less, and (4) measure the momentum transfer efficiency (β) of the impact and characterize the resulting effects of the impact. The data necessary to achieve these requirements will be obtained and analyzed by the DART Investigation Team. We discuss the rationales for the data to be gathered, the analyses to be undertaken, and how mission success will be achieved.

Unified Astronomy Thesaurus concepts: Asteroids (72); Asteroid satellites (2207); Near-Earth objects (1092); Impact phenomena (779)

1. The Double Asteroid Redirection Test: Overview

The Double Asteroid Redirection Test (DART) is a planetary defense demonstration mission to be launched by NASA and managed by NASA's Planetary Defense Coordination Office (PDCO). DART's launch is scheduled for 2021 November, arriving at the Didymos asteroid system in 2022 late September or early October, and culminating with an impact into the secondary of that binary system, (65803) Didymos I Dimorphos (referred to throughout the manuscript as simply "Dimorphos," and previously known in the literature by the temporary name "Didymos B"). The primary goal of the DART mission is to demonstrate the "kinetic impactor" (occasionally termed "kinetic deflector") as a viable technique for planetary defense. The kinetic impactor concept is to deflect an asteroid by ramming a mass into it at high speed, which sufficiently changes the asteroid's orbit. This technology is one that could be employed in the future to prevent an asteroid from impacting Earth. In this paper, we focus on the tasks that will be undertaken to meet DART's investigation goals described in Cheng et al. (2018).

The DART spacecraft will be supplemented by a 6U CubeSat named the Light Italian CubeSat for Imaging of Asteroids (LICIACube; Dotto et al. 2021). LICIACube is managed by the Italian Space Agency (ASI) and will be carried and deployed by DART to provide on-site documentation of the DART kinetic impact and immediate aftermath and contribute to DART's planetary defense investigation. LICIACube data will contribute to DART requirements for characterization of the Didymos system and the DART ejecta plume and, if possible, observation of the crater made by DART (Section 6). In addition, Hera, a European Space Agency rendezvous mission, will arrive 4 yr after DART's kinetic impact and perform a thorough assessment of the impact effects. Hera and its goals are described more fully in Michel et al. (2018).

1.1. Why Didymos?

The DART project is a descendant of ESA's Don Quijote mission concept (Wolters et al. 2011). In the Don Quijote concept, a rendezvous spacecraft would arrive at the target asteroid to perform initial reconnaissance observations, and a kinetic impactor would arrive while the rendezvous spacecraft remained nearby. Following the impact, the rendezvous spacecraft would assess the results. The costliness of a two-spacecraft mission prevented Don Quijote from being considered further by ESA. It was later recognized that targeting the secondary

member of an eclipsing binary asteroid system would allow the kinetic impactor experiment to be conducted with a single spacecraft through comparison of the secondary's orbit before and after the kinetic impact. This could be done via photometric light-curve measurements of the target system from Earth-based facilities by monitoring the timing of mutual events (occultations and eclipses by the system primary and secondary of one another) before and after the experiment (Pravec et al. 2006).

Roughly 60 binary near-Earth asteroids (NEAs) have been detected by radar, approximately 50 of which were known when study of the DART concept was begun (Margot et al. 2015). The accessibility of mission targets is often measured in "ΔV," which is related to the energy needed to reach an object. Didymos has a ΔV that makes it among the most accessible of these 60 NEA binaries. However, accessibility alone is not the sole discriminator of suitability. Binary targets with lower ΔV than Didymos have secondaries too large to be measurably deflected by the spacecraft masses under consideration, are poorly characterized in terms of physical and/or orbital properties, do not make close approaches to Earth for several decades in the future, are noneclipsing as seen from Earth for large stretches of their orbit, or have some combination of all of these factors. Didymos stands out as a well-characterized (De Léon et al. 2006; Pravec et al. 2006; Scheirich & Pravec 2009; Dunn et al. 2013; Naidu et al. 2020a), accessible asteroid binary system with an orbit conducive to measuring orbit changes via light-curve measurements, to which an efficient, affordable kinetic impactor demonstration mission can be sent, and from which meaningful results can be extracted without waiting decades for a suitable opportunity.

Using Didymos as the DART target system has an additional benefit. Analysis of the visible–near-IR reflectance spectrum of Didymos by Dunn et al. (2013) shows that its composition is consistent with the L/LL chondrites, the composition of the most common meteorite falls. Separate observations of the components of asteroid binaries of comparable size to the Didymos system have not been possible thus far, but leading models of asteroid binary formation predict that satellites form from material sourced from their primaries and should have similar if not identical compositions (Margot et al. 2015; Walsh & Jacobson 2015). One of the end states of tidal evolution in asteroid binary systems is the formation of an "asteroid pair," in which two objects share very similar heliocentric orbits without evidence of a collisional family (Vokrouhlický & Nesvorný 2008). Measurements of pairs show very similar spectral properties (Moskovitz 2012; Wolters et al. 2014; Pravec et al. 2019), consistent with the expectation that components of binary systems have similar compositions. Moreover, Pravec et al. (2006) found from analysis of depths of mutual events in binary near-Earth asteroids that albedos of both components of a binary NEA are the same or similar to within 20%. These findings give us confidence that Dimorphos's composition is very likely to also be L/LL chondrite. Thus, not only is the Didymos system the best choice for mission design and engineering reasons, but its components are also representative of likely potential impactors. Finally, Dimorphos, at roughly 165 m diameter, is close to (but above) the minimum size (140 m) for an object to be defined as a potentially hazardous asteroid (PHA). Given the nature of asteroid size–frequency distributions, smaller objects are far more numerous than larger ones, and therefore Dimorphos is of a typical size for the most common PHAs. Taken all together, these factors mean that the experimental results will be applicable to a large number of possible planetary defense scenarios.

1.2. DART Level 1 Requirements

Although DART is managed within NASA's Science Mission Directorate, as a planetary defense mission it differs from typical science missions such as those selected via the competitive Discovery or New Frontiers processes. Rather than a Science Team, DART has an "Investigation Team," reflecting the focus of the mission on the applied science of planetary defense. Nevertheless, the goals of DART involve scientific measurements, the studies carried out by the Investigation Team use typical scientific processes, and many of the planetary defense goals are aligned with fundamental science questions.

Like all missions, DART has a set of level 1 (L1) requirements that must be met in order for the mission to be considered a success. The four L1 requirements are listed below in their official forms, with the fourth requirement having two parts:

1. *DART-1.* DART shall intercept the secondary member of the binary asteroid (65803) Didymos as a kinetic impactor spacecraft during its 2022 September–October close approach to Earth.
2. *DART-2.* The DART impact on the secondary member of the Didymos system shall cause at least a 73 s change in the binary orbital period.
3. *DART-3.* The DART project shall characterize the binary orbit with sufficient accuracy by obtaining ground-based observations of the Didymos system before and after spacecraft impact to measure the change in the binary orbital period to within 7.3 s (1σ confidence).
4. *DART-4A.* The DART project shall use the velocity change imparted to the target to obtain a measure of the momentum transfer enhancement parameter referred to as "Beta" (β) using the best available estimate of the mass of Didymos B.
5. *DART-4B.* The DART project shall obtain data, in collaboration with ground-based observations and data from another spacecraft (if available), to constrain the location and surface characteristics of the spacecraft impact site and to allow the estimation of the dynamical changes in the Didymos system resulting from the DART impact and the coupling between the body rotation and the orbit.

Note that changes to the "binary orbital period" mentioned in the requirements refer to changes in the orbit of the secondary around the primary, not the orbit of the binary system around the Sun. Also note that the threshold DART mission fulfills L1 requirements 1 through 4A, and the addition of requirement 4B constitutes the baseline DART mission.

The studies carried out by the Investigation Team and described in the following sections are designed to ensure that the L1 requirements are met by characterizing the Didymos system via observations and simulations prior to, during, and after the impact period. Five working groups (WGs) have been defined within the Investigation Team, with a charge to coordinate and carry out work in Impact, Observations, Dynamics, Proximity Imaging, and Ejecta as they relate to the DART mission and the L1 requirements, as well as additional relevant work beyond what is strictly required, but that can extract additional value from the DART mission (Table 1). The tasks in Table 1 are further described below.

Table 1
Traceability of DART Level 1 Requirements to DART Investigation Tasks

DART Level 1 Requirements	Investigation Team Activities
DART-1: …intercept the secondary member of the binary asteroid (65803) Didymos...and DART-2: …cause at least a 73 s change in the binary orbital period.	Determine Didymos system properties (Observations WG)
	Model binary system dynamics (Dynamics WG)
DART-3: …obtaining ground-based observations of the Didymos system before and after spacecraft impact to measure the change in the binary orbital period to within 7.3 s (1σ confidence)	Determine Didymos system properties, measure change in orbital period (Observations WG)
DART-4A: …use the velocity change imparted to the target to obtain a measure of the momentum transfer enhancement parameter referred to as "Beta" (β) using the best available estimate of the mass of Didymos B.	Determine β from DART data (Impact WG)
	Determine the shape of Dimorphos (Proximity Imaging WG)
DART-4B: …constrain the location and surface characteristics of the spacecraft impact site and allow the estimation of the dynamical changes in the Didymos system resulting from the DART impact and the coupling between the body rotation and the mutual orbit.	Model the ejecta mass and crater size (Impact WG)
	Constrain dynamical evolution of ejecta from telescopic observations (Observations WG)
	Investigate dynamical effects of the DART impact (Dynamics WG)
	Model Ejecta from the DART impact through the near field and far field (ejecta WG)
	Constrain the impact location, determine Didymos system properties, characterize the impact site, and image the impact results (Proximity Imaging WG)

2. Requirements DART-1 and DART-2

The identification of Didymos as the best choice for a kinetic impactor demonstration (Section 1.1) leads naturally to requirements DART-1 and DART-2. Figure 1 shows the Earth–Didymos distance from 1996 (the year Didymos was discovered) to the end of 2069. The 2022 close approach provides the best future Earth-based observing conditions for Didymos until 2062; this drives the timing of the DART impact as required in DART-1. The 2022 approach is also the best opportunity for high-quality radar measurements until 2062 (Naidu et al. 2020a), although radar observations are not required to meet the DART L1 requirements. The properties of the Didymos system also drive the magnitude of the required period change in DART-2: the orbit period of Dimorphos is approximately 11.9 r (Pravec et al. 2006; Scheirich & Pravec 2009; Naidu et al. 2020a), or approximately 42,840 s. A period change sufficient to amount, after 1 month, to an orbit phase change of 10% relative to the unperturbed case was deemed observable. Dimorphos completes roughly 59 orbits in 29 days, meaning that the accumulated period change must amount to 4284 s (or 10% of the orbit period) in 59 orbits, or 73 s difference accruing per orbit (and thus a required 73 s change in orbit period).

The role of the Investigation Team for the first two L1 requirements can be summarized as ensuring that there is sufficient knowledge of the orbit and position of Dimorphos so that the DART spacecraft impacts Dimorphos and transfers enough momentum to cause the required change in period. This leads to two main tasks:

1. Determine Didymos system properties: There are several existing data sets that are being used in concert with newly obtained data to determine the properties of the Didymos system, both for establishing the unperturbed baseline state of the system and to aid in setting the arrival time for the DART spacecraft. Light-curve measurements of Didymos are available from 2003 and 2015–2021 (Pravec et al. 2006; Naidu et al. 2020b, 2021), with additional measurements planned in 2022–2023 before and after the time of impact (though the post-impact observations, along with observations sufficiently close to the impact, obviously cannot be used for targeting). Radar measurements from 2003 are also available (Naidu et al. 2020a).

The amount by which DART's arrival time can be changed after launch is a function of propellant and the time remaining before the arrival itself, among other factors. Given engineering considerations, a desire to limit propellant use for corrections, and the observability windows of Didymos, two requirements on the true anomaly knowledge of Dimorphos have been placed on the Investigation Team: $\pm 45^\circ$ (3σ) when extrapolated to the impact time, by 150 days prior to launch, and $\pm 15^\circ$ (3σ) when extrapolated to the impact time, by 55 days prior to the kinetic impact. The spacecraft has the opportunity of changing the arrival time by up to $\pm 60^\circ$ of true anomaly, or by roughly 2 hr, during a trajectory correction maneuver 40 days prior to impact.

In order for the DART spacecraft to impact Dimorphos, and to impart the largest change in the orbital period of Dimorphos with a given mass and trajectory, it is desired to impact Dimorphos as close as possible to head-on (i.e., near the center of its leading hemisphere), or alternately near the center of its trailing hemisphere. While the DART spacecraft is equipped with an on-board system that will autonomously target the

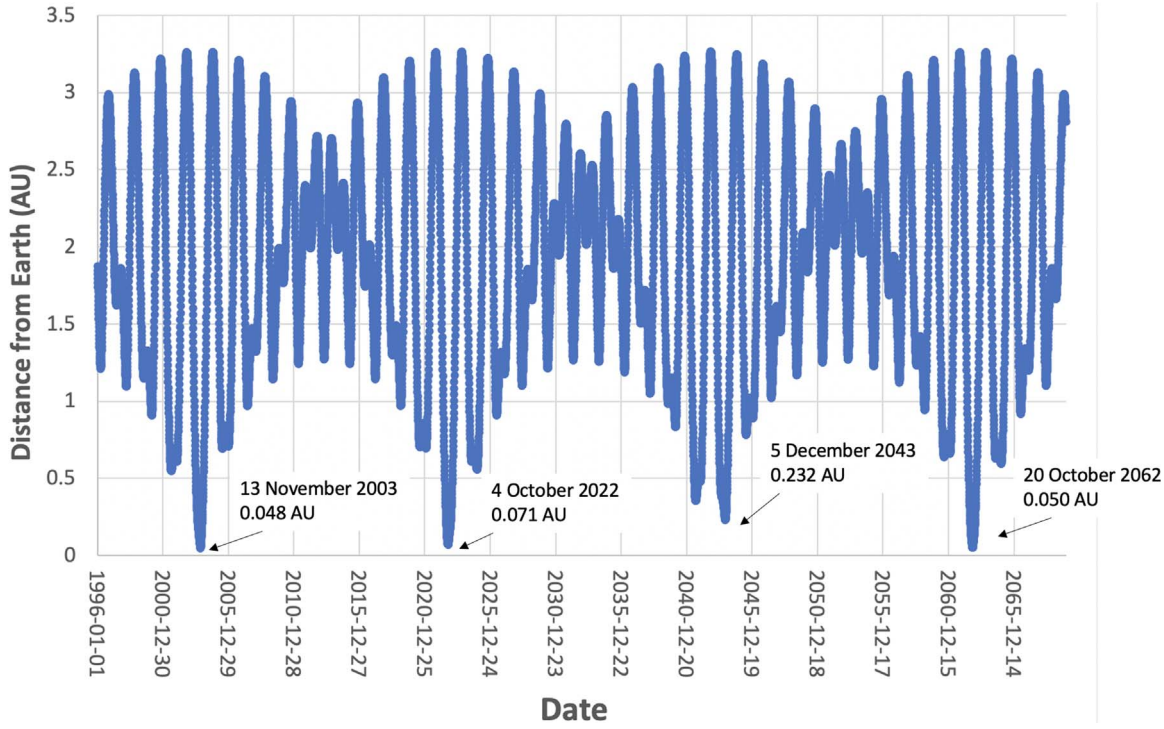

Figure 1. Distance between Didymos and Earth over time. Over the 75 yr span from the beginning of 1996 to the end of 2069, the Didymos system has three close approaches (<0.1 au) to Earth. The first of those was in 2003 and was a period of intense Earth-based characterization, including the radar measurements reported in Naidu et al. (2020a). The second close approach will be the DART impact epoch. After 2022, Didymos does not come within 0.1 au of Earth until 2062.

Table 2
Parameter Ranges for Possible DART Impact Dates

Parameter	Min	Max	Earliest	Latest
DART speed relative to Didymos (km s^{-1})	6.12	6.76	6.15	6.76
Angle between DART velocity and Dimorphos velocity	146.°55	169.°00	167.°83	146.°55
Component of angle between DART velocity and Dimorphos velocity in Dimorphos orbit plane	170°	180°	170°	180°
Angle between DART velocity and Dimorphos orbit plane	−33.°45	−6.°92	−6.°92	−33.°45
Angle between Dimorphos velocity and Dimorphos–Sun line	50.°75	61.°82	51.°50	59.°18
Earth–Dimorphos–Sun angle	51.°75	60.°64	51.°76	60.°63
Earth–Dimorphos–Didymos angle	126.°67	128.°70	128.°45	127.°62
Sun–Dimorphos–DART angle (solar phase angle)	58.°30	59.°98	59.°98	58.°53

smaller Dimorphos and not the larger Didymos, the timing of DART's impact needs to be arranged correctly to arrive in the Didymos system when such a direct leading-hemisphere impact is possible. Telescopic observations prior to the impact apparitions and analyses of those observations will provide crucial data about the position of Dimorphos about Didymos to make this determination of DART's impact timing. Operational requirements, including communications considerations and the availability of ground stations with lines of sight to DART, along with knowledge of the orbit phase of Dimorphos, will play a role in determining whether the arrival time (and thus arrival angle) will need to be altered slightly from a direct leading-side impact (Table 2). The exact launch date will set the trajectory to Didymos, which in turn will determine the set of arrival conditions (Figure 2).

2. Model binary system dynamics: The components of the Didymos–Dimorphos system are nonspherical and in close proximity compared to their sizes: Dimorphos orbits at 3.1 Didymos radii, with less than 730 m separating their surfaces not taking shape into account, which complicates the system's dynamics compared to a simple Keplerian two-body system. Modeling the dynamics of the Didymos binary system provides knowledge to inform the Design Reference Asteroid (DRA; Section 3.1 and Appendix A) and determination of the orbital properties. The dynamics modeling includes numerical simulations of the full two-rigid-body problem, characterized by fully coupled rotational and translational dynamics, applied to the Didymos binary asteroid system. This effort includes a sweep over parameter uncertainties to obtain a range of expected encounter circumstances (such as pre-impact libration state)

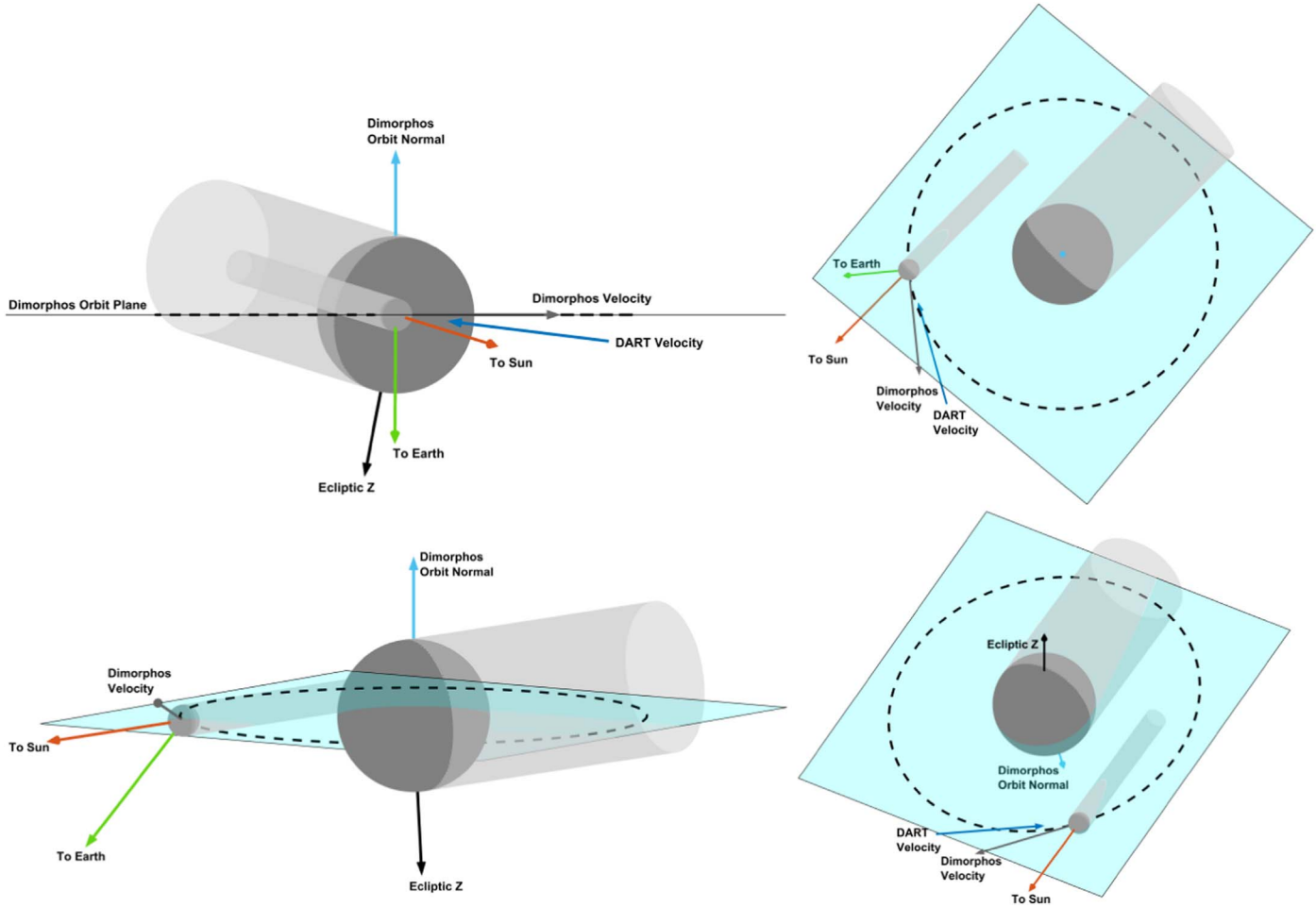

Figure 2. Geometry of DART Impact. Panels show the view from along the Didymos–Dimorphos line (top left), from above the system north pole (top right), from DART (bottom left), and from Earth (bottom right) at the final moments before the DART impact into Dimorphos. Included are the Dimorphos orbit plane and a schematic of the shadows cast by Didymos and Dimorphos.

and post-impact outcomes (such as deflection magnitude) as a function of momentum transfer efficiency.

Ignoring effects due to shape, topography, etc., the largest momentum transfer would occur when the angle between DART's incoming velocity vector and Dimorphos's instantaneous orbital velocity vector is 180°, that is, when there is a head-on collision. This ideal geometry has additional benefits in the specific case of the DART impact: such an impact will reduce the size of Dimorphos's orbit, shortening its orbit period. Because Dimorphos's orbit period is just shy of 12.0 hr, shortening the period ensures that the impact will not coincidentally leave the period at 12.0 hr and nearly resonant with Earth's rotation period, which would complicate the observing efforts necessary for DART-3. As noted, however, operational considerations may outweigh these observational benefits and may force a decision to use a trailing-side impact. Moreover, neither a precisely head-on nor precisely rear-end collision is achievable, as the incoming trajectory of DART will be out of the orbital plane of Dimorphos by as much as 33° (Table 2).

Extensive work has been done to investigate the extent to which the position of Dimorphos can be extrapolated into the future given its known state at an earlier time. Agrusa et al. (2020) report the results from this work, showing that the close proximity and specific shapes of the components of the Didymos system lead to non-Keplerian behavior and extreme sensitivity to initial conditions. For this reason, the pre-impact orbital phase of Dimorphos cannot be predicted from numerical simulations alone. However, the orbital phase prediction requirement can still be met with existing and future ground-based observations (See Section 2.1).

2.1. Observability of Didymos for DART-1 and DART-2

Save for imagery used for terminal guidance and to characterize the impact site, the data required to meet the L1 requirements can or must be acquired via astronomical measurements of the Didymos system. Because the components will not be optically resolved from one another save perhaps at close Earth approach in 2022 by the most capable adaptive optics systems, the following discussion uses values for both components combined. Figure 3 shows the observability of Didymos between 2020 and 2023 in terms of its solar elongation and brightness. Didymos reached a peak V magnitude (V) brightness of approximately 18.9 on 2021 February 18 and reached opposition 2 days later. It was well placed for northern hemisphere observatories during the 2020–2021 apparition. After spring of 2021, Didymos will be poorly placed for Earth-based observations until the DART impact apparition of 2022. The current best-fit solution for Dimorphos's orbit period, natural change in that orbit period,

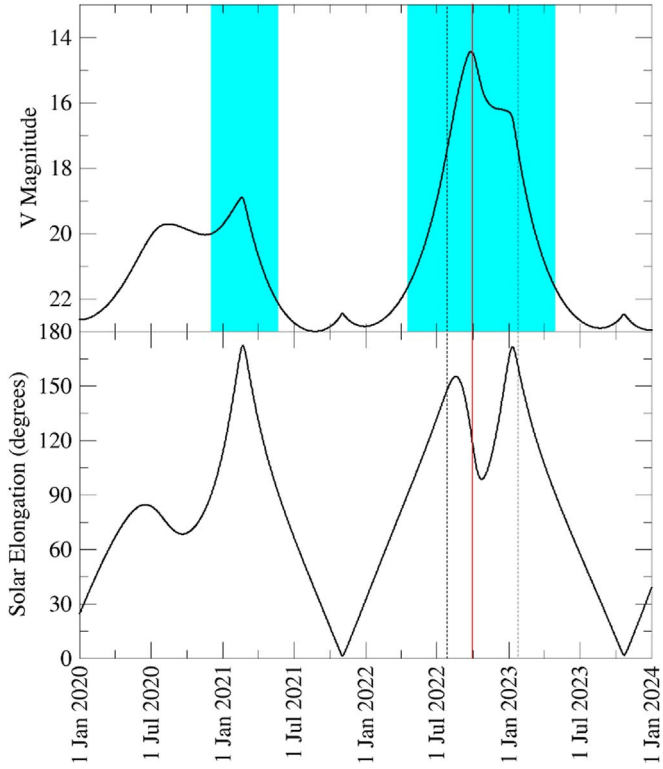

Figure 3. *V* magnitude (top) and solar elongation (bottom) for the Didymos system over 2020–2023. Note that the *y*-axis for the top panel is inverted to represent larger magnitudes being fainter. Didymos spends an extended period as a bright object at large solar elongations during the DART impact epoch in 2022–2023, with two separate oppositions. Shaded regions on the top panel represent periods when Didymos is >90° from the Sun. The solid red vertical line represents an impact date of 2022 September 30. The period between the two vertical dashed lines is the period when Didymos is brighter than $V = 17.5$ and meter-class telescopes can obtain data that can meet required photometric precision in typical conditions (Section 3.2.1).

and system standard gravitational parameter (GM) is presented in Table 3. The small but nonzero natural change in orbit period is consistent with, and interpreted as, being due to the binary YORP torque (BYORP; Cúk & Burns 2005; Cùk & Nesvorny` 2010), caused by unbalanced thermal emission in binary systems, which would lead to an additional change in Dimorphos's mean anomaly proportional to the square of time.

The Investigation Team is conducting light-curve observations, using both guaranteed telescope access supported by the DART project and the standard competitive proposal process, to ensure meeting the DART-1 and DART-2 requirements.

3. Requirement DART-3

The investigations to support L1 requirement DART-3 are observationally based. Two tasks fall on the investigation team to address this requirement:

1. *Determine Didymos system properties.* This task is the same as detailed in Section 2 to support DART-1 and DART-2. In addition to providing knowledge of the location and orbit and rotation period of Dimorphos, along with estimates of its size, composition, and shape, knowledge of the Didymos system is needed prior to the impact event in order to be able to determine the change imparted by DART.

Table 3
Current Solutions for Dimorphos Orbit Period

Parameter	Value
Period (hr)	11.921 628 7 ± 0.0000031
$\dot{n}$ (deg yr^{-2})	0.13 ± 0.03
GM (m^3 s^{-2})	37.036

2. *Measure change in orbital period.* Telescopic observations after the DART impact will enable the change in the orbital period of Dimorphos to be determined. Multiple observatories will be under contract with the DART project to ensure support for this critical measurement. An international observing campaign to synergistically contribute additional data to the DART mission is planned but is not necessary for meeting mission requirements.

3.1. Determine Didymos System Properties

Our current knowledge of the nature of the Didymos system is captured in the "DRA." The DRA currently has 43 fundamental and derived physical and orbital parameters to serve as a basis for common input to Investigation Team simulations and studies (see Appendix A). The DRA was originally implemented as a text document but has been adapted to be an online database that can be queried by DART team member applications throughout the mission. The DRA is to be updated as appropriate with each observing season, with the final pre-DART impact version scheduled to be complete in 2021 September, and post-impact DRA updates scheduled for release in 2022 October, November, and December, with release of the final post-impact DRA scheduled for 2023 April. Team members have access to the current DRA via the project Science Operations Center. The current DRA at the time of this writing is included as Tables A1–A6 in Appendix A. Later versions will similarly be included in future publications by project team members.

3.2. Measure Change in Orbital Period

As with DART-1 and DART-2, telescopic measurements of Didymos's light curve will be used to meet the DART-3 requirement. As seen in Figure 3, Didymos will brighten throughout the first 9 months of 2022. On 2022 July 1 Didymos's *V* magnitude becomes brighter than 19.0, where it will remain until 2023 February 18, well after DART's kinetic impact. Didymos will reach a local maximum in solar elongation of 155° on 2022 August 18, after which solar elongation will decrease. It will reach a maximum brightness of *V* magnitude 14.4 on 2022 September 26–27. It will continue to draw closer to Earth for several days after reaching maximum brightness, with a closest approach distance of 0.071 24 au (10.66×10^6 km) on 2022 October 4. However, because of Didymos's increasing phase angle in the days before close Earth approach, its brightness decreases despite the decreasing distance.

Didymos remains at solar elongations of approximately 100°–130° between 2022 September 22 and December 5, spanning the pre- and post-impact period, and during which period its brightness remains at *V* magnitude <16.2. During

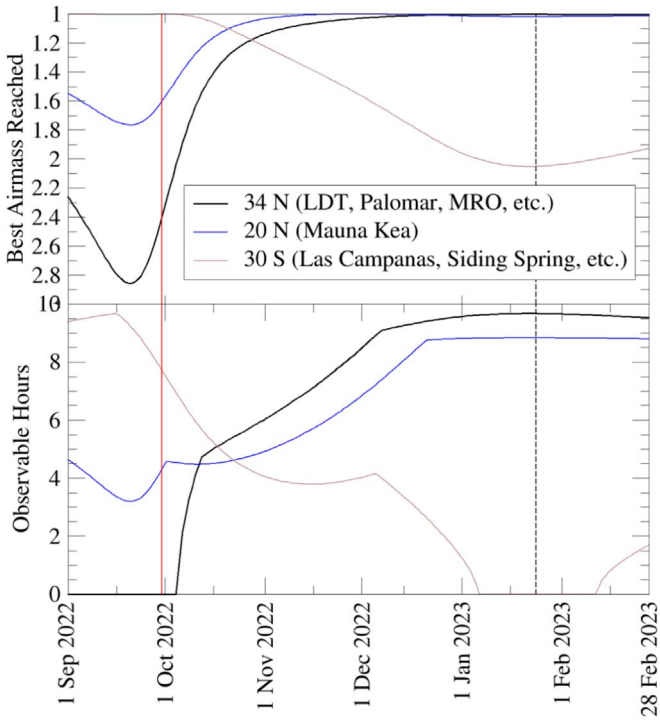

Figure 4. Best air mass (astronomically defined as the secant of the zenith angle, so air mass overhead = 1.0) reached by Didymos (top) and the number of hours above 30° elevation (i.e., air mass <2) for three latitudes during the DART impact apparition. These latitudes are representative ones for southern hemisphere observatories (30°S), Hawaiian observatories (20°N), and the observatories of the U.S. Southwest (34°N). As in Figure 3, the dashed line marks the time after which Didymos is fainter than $V = 17.5$, Early in the apparition, observations from Las Campanas (and other observatories at similar southern latitudes) are best, with Didymos spending long periods high in the sky. By late October, northern hemisphere observatories have observing circumstances as good as southern hemisphere locations and are better sites for Didymos observations through late 2022 into early 2023.

that span, it moves from a mid-southern decl. of −35° (well placed for southern hemisphere observatories, nonideal for Hawaii, and difficult from other northern hemisphere observatories) to a decl. of +22° (well placed for northern hemisphere observatories, less ideal for southern hemisphere observatories). Figure 4 shows the number of hours per night Didymos is observable and the minimum air mass it reaches for different observatories on selected dates over 2022–2023. The interplay of Didymos's east–west and north–south motions across the sky, its changing solar elongation, and the seasonally changing lengths of nighttime in different locations lead to the detailed behavior of the specific curves in Figure 4.

The properties of interest to the Investigation Team include not only the binary orbit period and semimajor axis but also its other Keplerian orbital elements. Unlike the measurements that will constrain BYORP, the measurements that constrain or determine the inclination, eccentricity, etc., are not required to ensure that DART impacts Dimorphos and therefore are of lower priority.

As noted above, Didymos's position in the sky changes throughout the impact apparition, with northern and southern hemisphere observatories having different ideal observing times. To account for this, and as mentioned in Section 2, the DART project plans to support telescopes in both hemispheres that are operated by US-based institutions (Figure 4), covering a range of sizes: the Baade and Swope telescopes at Las Campanas Observatory in the south, Magdalena Ridge Observatory and the Lowell Discovery Telescope (LDT) at Lowell Observatory in the north, and the Las Cumbres Observatory network in both hemispheres, including a site in Hawaii.

3.2.1. Photometry

If the minimum requirement for orbital period change (73 s) is met, the length of Dimorphos's period will differ from the unperturbed case by roughly 0.17%, and every orbit Dimorphos will accrue an additional 0.17% difference in mutual event timings due to this change. While 73 s is the minimum required change, the specifics of the DART impact lead us to suspect that a 5-to-10-minute change is more likely, if still a conservative expectation (Cheng et al. 2018). A 7-minute change in period corresponds to a 1% change relative to the unperturbed period, etc. Figure 5 schematically shows how the change in orbit period caused by the DART impact will accrue in Didymos's light curve, with only the mutual events shown and the variation due to the rotation of Didymos removed, and neglecting effects due to changing viewing angles between the Sun, the fixed stars, the observer, and the Didymos system. After 15 orbits (roughly 7 days after the impact), the 73 s period change results in a timing offset of the mutual events from the unperturbed case by approximately 18 minutes, with the 7-minute orbit period change accruing a 1.7 hr offset. Note that Figure 5 assumes a leading-hemisphere impact that shortens the orbit period of Dimorphos. A trailing-hemisphere impact that lengthens the orbit period of Dimorphos will have similar offsets, but with mutual events later than the unperturbed case.

In practice, it is unlikely that a very short campaign on any telescope can reach the 7.3 s uncertainty required of the measurement of the new orbit period. However, a relatively short campaign should be able to obtain the minimally required data: the photometric data used to discover Dimorphos (Pravec et al. 2006) spanned 13.2 days in 2003 November–December, with analysis by Scheirich & Pravec (2009) resulting in a precision of $+14/-22$ s (3σ). These data were taken from four different observatories with aperture sizes ranging from 0.35 to 1.5 m. Note that this 3σ uncertainty is roughly comparable to the required 7.3 s 1σ uncertainty for DART-3.

The Investigation Team has been using as guidelines for usable data a cadence of ∼3 minutes between images, with signal-to-noise ratio (S/N) of >50 (and S/N > 100 preferable). If S/N > 100 can be met with exposure times <2 minutes, improved S/N is preferred to a faster imaging cadence. Online exposure time calculators (for instance, the one hosted by the Las Cumbres Observatory: https://exposure-time-calculator.lco.global/) show that S/N ∼ 100 can be reached on a 1 m telescope in 120 s integrations for objects at $V = 17.5$ at air mass 1.3 and a quarter-moon phase, with S/N ∼ 50 reachable in the same conditions for $V = 18.4$. Didymos is brighter than $V = 18.4$ from 2022 mid-July to 2023 February and brighter than $V = 17.5$ from late 2022 July to late 2023 January, though of course much of those time periods are after the impact.

During the 2003 apparition, Didymos was at V magnitude ∼12.8–13.2, roughly 1.5 mag (factor of 4) brighter than it will be shortly after the impact, and roughly 3 mag (factor of 16) brighter than it will be a month after the impact. To make up for these differences using larger apertures alone requires mirrors ∼2–4 times larger in diameter than were used at that apparition,

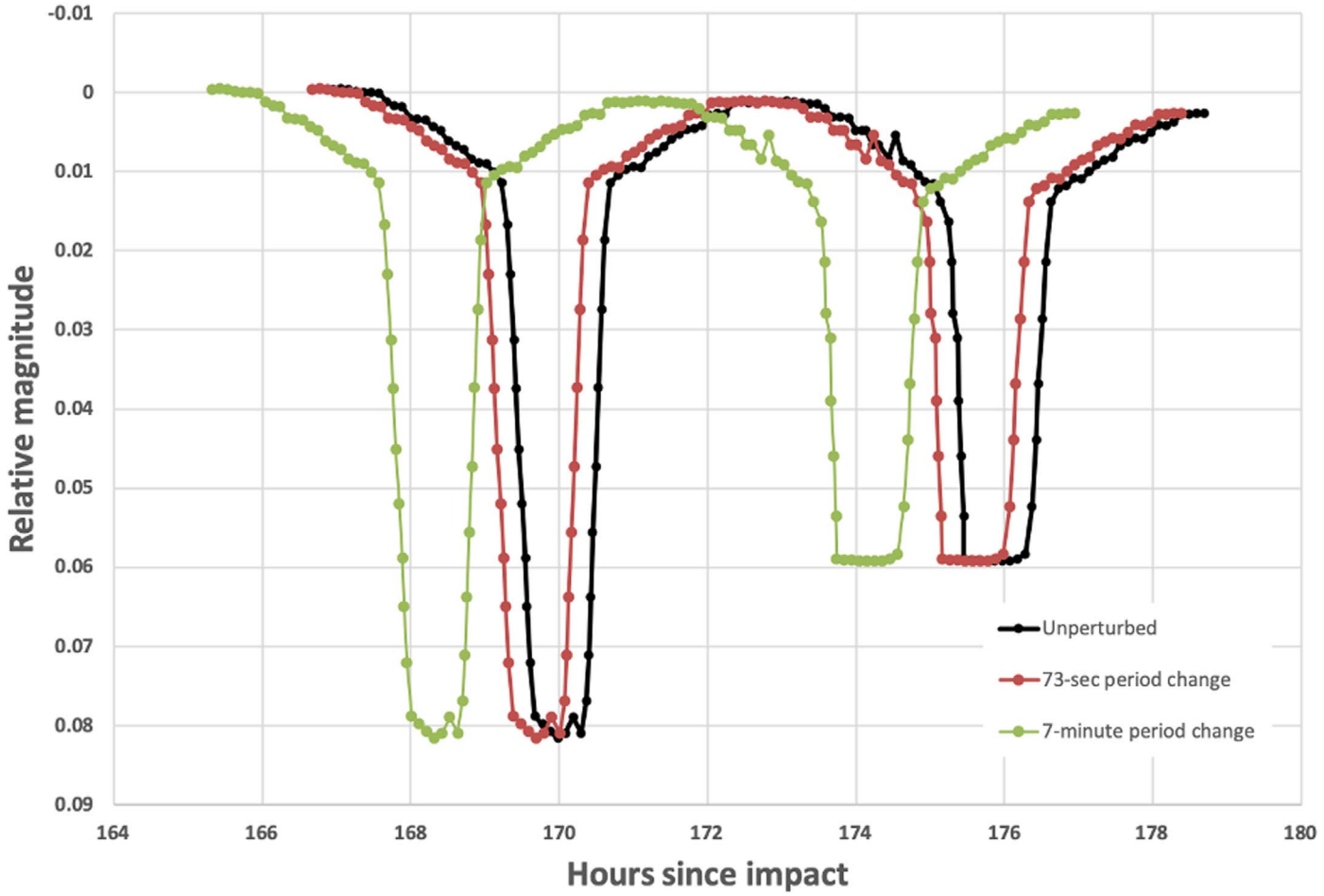

Figure 5. Schematic offset between the mutual events in the unperturbed Didymos system light curve and light curves from 73 s and 7-minute period changes, as seen 15 orbits following a leading-side ("head-on") DART impact. There is a roughly 18-minute difference between the timing of the mutual events of the unperturbed system and the minimum required 73 s period change case, easily detectable given expected data. The 7-minute period change leads to an even larger offset.

or ∼1–6 m. The observatories to be supported by the DART project are in this size range, including the 4.3 m LDT, the 6.5 m Magellan Telescopes, and the 2.4 m Magdalena Ridge Telescope. Simulations were undertaken by Scheirich et al. (2019) assuming rms uncertainties of 0.01 mag, with the conclusion that observations of four mutual events per month (a small fraction of the ∼60 mutual events that occur each month in the Didymos system) beginning on 2022 October 15 should result in an orbital uncertainty of ±10 s (3σ) by the end of November 2022 and ±4 s by the end of 2023 January, with the 1σ L1 requirement met during November. Higher-quality photometry, as would be expected from apertures larger than 1 m aperture, and/or additional mutual event measurements will further shorten the time until the requirement is met and reduce the uncertainty of the final measurement of Dimorphos's orbit period.

While the DART project will only support a limited number of observatories, we expect astronomers around the world, particularly those involved in the Hera mission, to be interested in participating in the 2022–2023 Didymos observations. These observations will be of great use to the DART project by providing different lines of sight to the Didymos system, providing additional margin against the threat of long-term regional weather problems, and allowing for monitoring of short-term variation in ejecta cloud brightness and morphology (if present).

3.2.2. Radar

Radar studies of Didymos were a key aspect of characterizing the system. Naidu et al. (2020a) detail the 2003 experiments and discuss the radar opportunities in 2022. New radar measurements are not necessary to meet the L1 requirements and are therefore not being directly supported by DART. But if radar observations are conducted, the highest-S/N observation opportunities from Goldstone will span the period of 2022 October 2–16, just following the nominal impact date of 2022 September 26. The spatial resolutions achievable from Goldstone will be 150 m pixel^{-1} if monostatic, improved to 75 m pixel^{-1} if bistatic measurements with the Green Bank Telescope are made. While these resolutions may only provide very coarse shape information, this level of astrometric precision could potentially reveal the orbit phase difference from the unperturbed case: Naidu et al. (2020a) calculate that a 1% change in Dimorphos's orbit period (or ∼7 minutes) would result in a ∼140 m day^{-1} change in the secondary's orbital position relative to the unperturbed case, which could be detected within a few days with Goldstone measurements. While a 1% change in period is much larger than the required change, it is consistent with what is expected from the DART impact. Thus, radar observations could provide an additional means of measuring the DART impact results that is independent of light-curve measurements.

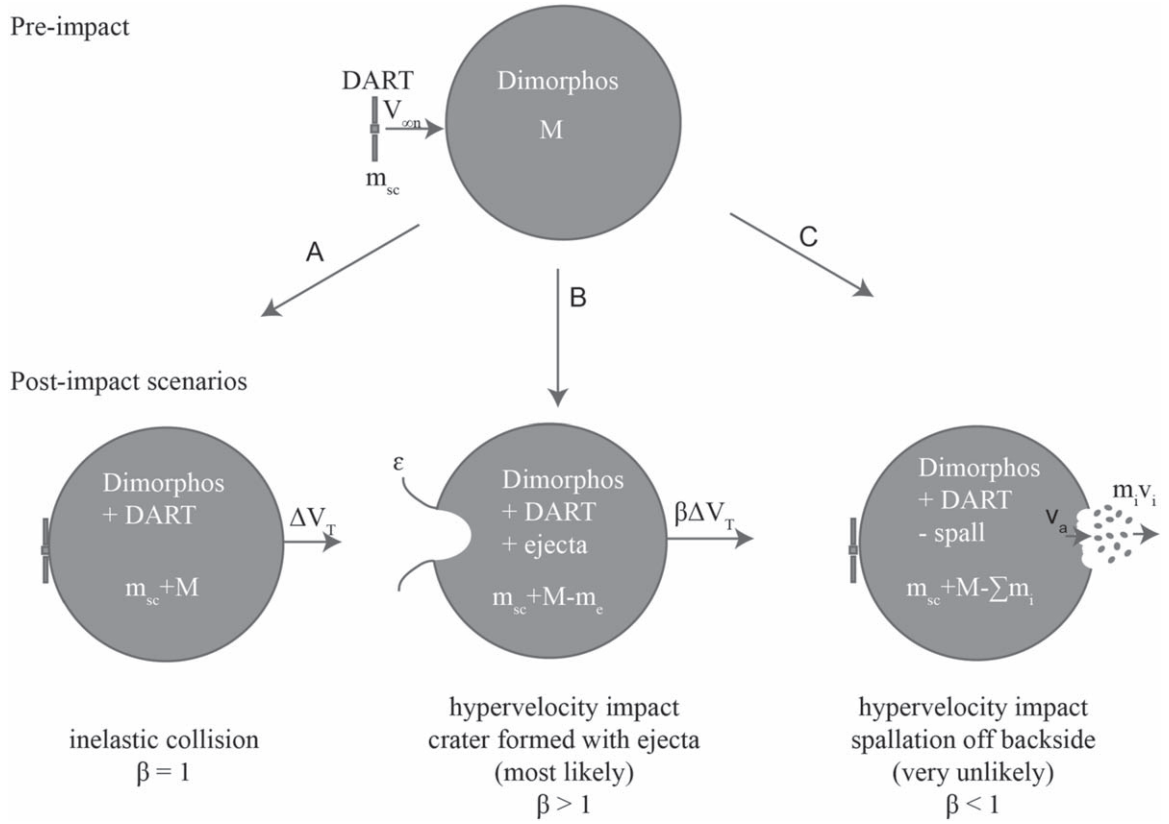

Figure 6. Possible scenarios post DART impact. (A) Slow-speed or inelastic collision adds DART's momentum to the asteroid, $\beta = 1$. (B) Hypervelocity impact creates a crater and results in ejecta being thrown off asteroid, which acts to increase momentum of the asteroid system, $\beta > 1$. (C) In a very unlikely case, spallation on the backside of the asteroid after the collision could act to more than counteract the momentum enhancement from the spacecraft, resulting in $\beta < 1$.

4. Requirement DART-4

The final requirement, DART-4, is split into a "threshold" requirement (DART-4A) and a "baseline" requirement (DART-4B). The threshold requirement uses data that are required to be obtained to fulfill DART-1, DART-2, and DART-3, while the baseline requirement takes advantage of additional data and analysis, including data returned from LICIACube. We describe DART-4A and DART-4B separately below, but both concern the momentum transfer efficiency factor, β.

In order to determine β, the momentum of Dimorphos prior to the impact must be compared to its post-impact momentum, while knowing the momentum carried along by DART itself. A significant part of the momentum change is expected to be due not to the momentum delivered directly by DART but to that carried by ejecta (Figure 6). Furthermore, impact simulations show that the momentum carried by the ejecta is a complicated, time-dependent, nonlinear function of impact angle, surface geology, topography, and the combined system dynamics, and the ejecta momentum vector need not be coplanar with the plane defined by the surface normal and incoming spacecraft velocity (e.g., Holsapple & Housen 2012; Scheeres et al. 2015; Syal et al. 2016).

5. Requirement DART-4A

The DART-4A Level 1 requirement is related to using the results of the DART impact to obtain a measurement of the momentum transfer enhancement parameter Beta (β). Appendix B details the definition of β in both idealized and more practical cases, as well as how DART will measure it. The Investigation Team has two main tasks to support this requirement:

1. *Determine the shape of Dimorphos.* An important component to determining β is knowing the mass of Dimorphos. DART will not measure the mass of Dimorphos directly, but spacecraft imaging will be used to constrain the shape and volume of Dimorphos, and a mass estimate will be derived using an appropriate assumption for the density (Section 5.2).
2. *Determine β from DART data.* The determination and interpretation of β combine the efforts of multiple Investigation Team working groups. β is a nonlinear function of several input factors (Appendix B), some of which could vary significantly from one object to another. In order to gain the most benefit from the DART experiment and be able to appropriately generalize its results to other scenarios, the relative importance of those input factors must be understood. Benchmarking of impact modeling codes (e.g., Stickle et al. 2020), followed by application of the codes to a variety of potential DART scenarios prior to impact, ensures that the team is ready to receive multiple inputs from the DART impact and use those inputs to determine and interpret the DART-produced β value.

5.1. Measuring the Shape of Dimorphos

The imaging time line for DART consists of three phases (Barnouin et al. 2019b):

Figure 7. This image of Itokawa provides an example of the highest resolution required for DRACO images of Dimorphos, which will be used as input into shape models, as well as used to determine the location and geology of the impact site. Dimorphos's diameter is estimated to be roughly 1/3 of Itokawa's long axis. The highest-resolution images planned for return will have roughly 23 cm pixel^{-1}, and the return of images with still-higher resolution is possible. Image credit: JAXA.

(1) *Approach phase*. This phase provides light curves at viewing geometries complementary to those obtainable by ground-based telescopes. It begins when the Didymos system is first detected by Didymos Reconnaissance & Asteroid Camera for OpNav (DRACO), about 30 days before impact. The Didymos system will not be resolved during most of this phase. Using approaches employed in previous efforts (Pravec et al. 2006; Viikinkoski et al. 2015; Weaver et al. 2016), these light curves will be used to tighten constraints on the rotation rate and shape of Didymos and the orbital period and shape of Dimorphos. The long-range images also will be used to search for additional satellites.

(2) *Terminal phase*. The terminal phase begins when the spacecraft initiates autonomous navigation a few hours prior to impact. During roughly the last hour of this phase, Didymos and Dimorphos can be separately resolved, and DRACO images support both autonomous navigation and asteroid characterization. By the end of this phase, images of Dimorphos will have a pixel scale of roughly 3.5 m.

(3) *Final phase*. The final phase comprises the last 4 minutes of the DART mission. In the current baseline plan with an impact velocity of 6.6 km s^{-1}, at 15 s prior to impact, DRACO will image Dimorphos with a pixel scale $\leqslant$50 cm. Higher spatial resolution data will continue to be acquired in the final seconds of the mission. Planned real-time DSN coverage enables downlink of the images acquired up to 7 s before impact (which will have 23 cm pixel scale in the baseline trajectory), and possibly including even higher-resolution images acquired during the final 7 s prior to impact. Because the impact velocity depends on the actual launch date, the time at which these pixel scales are met could shift by 1–2 s in either direction.

Images from DRACO will provide the main data sets for a shape model for Dimorphos and impact-site images with a spatial resolution of 66 cm pixel^{-1} or better (Figure 7). These data will be augmented by Earth-based light-curve data to develop a shape model of Dimorphos using stereophotoclinometry (Gaskell et al. 2008; Barnouin et al. 2020). Imaging along the incoming path for DART does not provide much opportunity for stereo or illumination variation, or for seeing more than half of the surface; nonetheless, initial modeling done by Barnouin et al. (2019b) demonstrates that volume uncertainties of 22% can be achieved from simulations of DART approach imagery using the shape of Itokawa, without any input from LICIACube or other non-DRACO sources (Figure 8). Bodies that are more symmetrical than Itokawa would yield smaller uncertainties. Inclusion of LICIACube data will provide stereo imagery and limb measurements that will not otherwise be available and will further improve the uncertainty on a volume estimate (and thus Dimorphos's mass estimate), but the exact amount is dependent on the shape of Dimorphos. A suite of simulations are currently underway to investigate this question in more detail. The shape model developed for Dimorphos will then be used, along with density estimates based on compositional analogs and a porosity estimate based on other asteroidal satellites (Section 5.2, Table 4), to provide an estimate of its mass and an associated uncertainty.

5.2. Mass Estimate for Dimorphos

Obtaining a measure of β, even in a simplified, idealized case, requires a measure of the mass of Dimorphos. While it is a goal of the Hera mission to make a measure of that mass to better than 10% in 2027 (Michel et al. 2018), the DART investigation will initially rely on a mass estimate based on the density of compositional analogs and the shape of Dimorphos.

The spectrum of the Didymos system was first reported by Binzel et al. (2004), who classified it as an Xk-class object based on 0.5–1.0 μm spectroscopy. Observations to 2.5 μm were made by de Léon et al. (2006), showing the presence of 1 and 2 μm silicate absorptions typical of S-complex asteroids. Dunn et al. (2013) analyzed the spectrum of Didymos and found it to be most consistent with an L/LL-chondrite composition. Theoretical and observational evidence suggests that asteroid satellites should share the same composition as their primaries (Margot et al. 2015), and therefore we expect Dimorphos to have the same composition as Didymos (Section 1.1). The Dunn et al. analysis, which supersedes that of a simple taxonomic classification, suggests that the components of the Didymos system would have a density of 3520–3580 kg m^{-3} if neither component has any porosity (Flynn et al. 2018). The mutual orbit period of Dimorphos and the sizes of the system components give a density for the system of 2170 ± 350 kg m^{-3} and an implied porosity of $38\% \pm 6\%$ (Naidu et al. 2020a), though the size difference between Didymos and Dimorphos (derived from the depth of dimming during mutual events and independently constrained by radar measurements) suggests that >95% of the mass resides in Didymos, and this density is most accurately thought of as a density for that object alone. There are few asteroid systems with available densities for both primary and secondary, and situations where the secondary is denser and where it is less dense both exist (Ostro et al. 2006; Naidu et al. 2015), though recent work on the light curve of (66391) Moshup suggests that its satellite Squannit may be significantly larger (and thus less dense) than the results from radar measurements (Scheirich et al. 2021). Geophysical limits on the density of Dimorphos can be calculated: the fact that it is in its current orbit without being tidally disrupted sets a minimum density if it is cohesionless. However, Zhang et al. (2017) found that Didymos is spinning faster than the critical limit for its nominal density, concluding that it probably has surface cohesion, which might imply that Dimorphos also has cohesion. The fact that no reflex motion in Didymos was seen

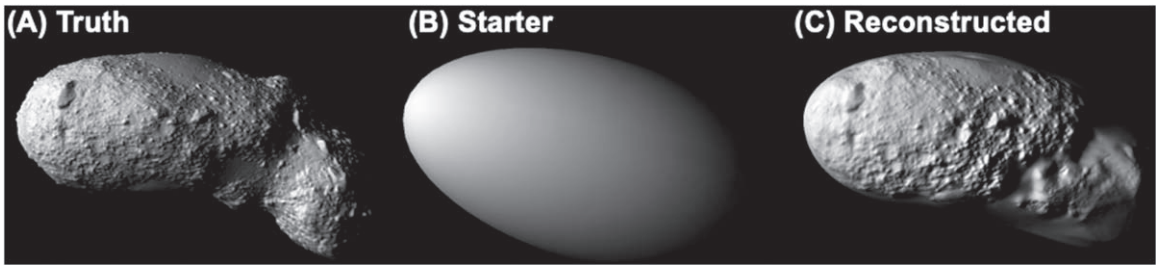

Figure 8. Uncertainty in the shape model can be estimated by simulating what would be calculated if Dimorphos were shaped like Itokawa, and comparing to a scaled-down, "truth" Itokawa shape model. The process under development for DART combines light-curve-derived ellipsoids with resolved images. The reconstruction case shown above returns a volume within 22% of the true shape. Additional data sources will further reduce this uncertainty.

in the 2003 radar measurements sets a maximum mass, and the fact that the compositional analog cannot have negative porosity sets a maximum density limit. Table 4 presents density constraints for Dimorphos that can be used to constrain its likely mass value.

5.3. Determining β from DART Data

The momentum transfer efficiency, β, is defined as the ratio of the change in the asteroid momentum to the momentum of the impacting spacecraft, in the direction perpendicular to the asteroid's surface at the point of impact. Appendix B explains the background of this definition (for more detailed discussion, see, e.g., Jutzi & Michel 2014; Scheeres et al. 2015) and also lays out the mathematical formalism for how β will be determined from DART data. Figure 6 shows schematically the possible outcomes of the DART kinetic impact and how they correspond to different values of β. A purely inelastic collision where all of the spacecraft momentum and energy are simply absorbed by the asteroid corresponds to $\beta = 1$. An increased momentum change due to the recoil from ejecta blown back along the spacecraft trajectory corresponds to $\beta > 1$, and a decreased momentum change caused by material spalled off from the opposite side of the asteroid, albeit unlikely, would correspond to $\beta < 1$.

An exact equation for β, developed in Appendix B, is

$$\beta = \frac{\frac{M}{m_{sc}}\Delta V_T - \boldsymbol{V}_{\infty_{\perp n}} \bullet \hat{\boldsymbol{e}}_T + V_{\infty_n} \boldsymbol{\epsilon} \bullet \hat{\boldsymbol{e}}_T}{V_{\infty_n}(\hat{\boldsymbol{n}} + \boldsymbol{\epsilon}) \bullet \hat{\boldsymbol{e}}_T}, \quad (1)$$

where M is the target mass, m_{sc} is the kinetic impactor (spacecraft) mass, $\hat{\boldsymbol{e}}_T$ is the unit vector in the direction of the satellite orbital velocity at impact, ΔV_T is the component of the satellite's velocity change in the direction of $\hat{\boldsymbol{e}}_T$, $\hat{\boldsymbol{n}}$ is the surface normal vector at the impact site, V_{∞_n} is the component of impactor velocity in the direction of the surface normal, $\boldsymbol{V}_{\infty_{\perp n}}$ is the component of impactor velocity orthogonal to the surface normal (that is, along the surface), and $\boldsymbol{\epsilon}$ is an offset vector between the surface normal direction and the ejecta momentum vector.

The inputs to Equation (1) can be separated into three categories, each the focus of a different working group: (1) estimate of tangential (along-track) change in orbital speed (ΔV_T: Observations Working Group); (2) estimate of Dimorphos shape and mass and impact location and surface normal at impact location (M and $\hat{\boldsymbol{n}}$: Proximity Imaging Working Group); and (3) estimate of off-normal component of ejecta momentum ($\boldsymbol{\epsilon}$: Impact Working Group). The other variables in Equation (1) are m_{sc}, $\hat{\boldsymbol{e}}_T$, and the components of $\boldsymbol{V}_\infty$. The DART spacecraft team will provide initial inputs of the spacecraft trajectory and system to the Investigation Team as a whole within a week after impact. In particular, the true anomaly of Dimorphos at the time of impact, which provides $\hat{\boldsymbol{e}}_T$, will be determined by the Navigation Team in conjunction with the Proximity Imaging Working Group, using DRACO images.

1. Estimate of tangential change in orbital speed (ΔV_T). As discussed for DART-3, the Observations Working Group will determine the change in the orbital period of Dimorphos that results from the DART impact. The period change determination will provide the change in velocity to Dimorphos as a result of the DART impact to use in the determination of β, as further detailed in Equation (5) of Appendix A. The final determination of the period change will use all available data from the 2022–2023 Didymos observing period and will be available by 2023 April. However, preliminary estimations of the period change will be available earlier for DART team use, starting at roughly 2 weeks after impact.

   Determining the change in orbit period is, besides an independent L1 requirement, a key input to the determination of β discussed in the following sections. Dimorphos travels around Didymos at an average speed of 174.2 mm s^{-1} (using the current DRA values). We expect a change of semimajor axis of roughly 10 m, with exact values dependent on the arrival mass of DART and the mass of Dimorphos. This estimate assumes a completely inelastic collision ($\beta = 1$) but assumes that DART's entry angle is 15° relative to Dimorphos's orbit plane. Those changes would lead to a new average speed of 173.5 mm s^{-1} and a ΔV of roughly 0.7 mm s^{-1}. A 7.3 s uncertainty (1ρ) is roughly 1.4% of the nominal period change, so we do not expect uncertainties in the orbit period to be a significant contributor to uncertainties in β.
2. *Estimate of Dimorphos shape* ($\boldsymbol{M}$ and $\hat{\boldsymbol{n}}$). As discussed in the previous section, spacecraft images will be used to produce a shape model of Dimorphos. The Proximity Imaging Working Group will produce an initial version of the shape model along with a volume determination within a month after the DART impact. This volume estimate will be used along with assumptions for the density of Dimorphos (Table 4) to estimate the mass of Dimorphos. Using spacecraft images, the local tilts and geology of the impact location will be determined to provide an estimate of the surface normal of the DART impact location, though information beyond determining the shape of Dimorphos is considered part of the efforts to achieve L1 DART-4B. It is expected that determination of the impact location and development of the

Table 4
Mass Constraints or Estimates for Dimorphos

Constraint or Assumption	Value	Implied Density for Dimorphos	Reference
If same density as Didymos	2170 ± 350 kg m^{-3}	2170 ± 350 kg m^{-3}	Naidu et al. (2020a)
Relative range of measured asteroid satellite densities	*(66391) Moshup*: secondary may be 40% denser than primary (see text); *(185851) 2000 DP107*: secondary is 25% less dense than primary	2170 ± 870 kg m^{-3} (non-Gaussian uncertainties)	Moshup: Ostro et al. (2006), Scheirich et al. (2021) DP107: Naidu et al. (2015)
Fluid object at Roche limit	Object exists in orbit with semimajor axis = 1190 m	>1150 kg m^{-3}	
No reflex motion seen in 2003 Didymos radar data	Reflex motion <15 m, with partial orbital coverage	<3000 kg m^{-3} if full orbit had been covered	Naidu et al. (2020a)
Grain density of compositional analog (zero macroporosity)	3520 ± 10 kg m^{-3} (LL average) 3580 ± 10 kg m^{-3} (L average)	<3580 ± 10 kg m^{-3}	Flynn et al. (2018)

Dimorphos shape model will occur in tandem. The surface area over which $\hat{\boldsymbol{n}}$ is determined should be roughly that of the DART spacecraft (Barnouin et al. 2019a), and work is underway to determine the extent to which the solar panels affect DART's effective surface area (Owen et al. 2019). DRACO images will be able to support calculation of surface normals for length scales of roughly 1 m and larger, finer than will be necessary for these purposes.

3. *Estimate of off-normal direction of ejecta momentum ($\boldsymbol{\epsilon}$).* Ejecta formation and evolution have a profound influence on the value of β. The amount and trajectory of ejecta generated following impact depends nonlinearly on, e.g., impact incidence angle, target material properties, surface block distribution and frequency, and object shape. High-fidelity impact simulations provide information about the mass and velocity distributions for the ejecta, from which the ejecta motion can be determined. The Impact Working Group is performing suites of high-fidelity impact simulations to provide constraints on the magnitude of various unknowns (e.g., material properties, impact angle, block distribution) on ejecta generation and material trajectories (e.g., Stickle et al. 2015, 2017, 2020; Syal et al. 2016; Raducan et al. 2019, 2020; Rainey et al. 2020). These simulations utilize a variety of different standard impact hydrocodes (e.g., Stickle et al. 2020). In general practice, impact modelers on the Investigation Team simulate the DART impact in a plane containing the spacecraft momentum vector and the surface normal ($\boldsymbol{V}_\infty$ and $\hat{\boldsymbol{n}}$), with an assumption that the net ejecta momentum vector is coplanar. This assumption reduces the problem to a 2D calculation and allows consistency between simulations despite the fact that topography at the impact location is not known prior to receiving approach images, and thus the actual incidence angle with respect to the surface normal is uncertain. Focused 3D modeling by the Investigation Team will test this assumption in realistic DART impact cases. Both sets of simulations will be used to estimate the direction of the ejecta momentum vector in the actual DART impact and determine the difference between this direction and the surface normal $\hat{\boldsymbol{n}}$, denoted as $\boldsymbol{\epsilon}$.

Figure 9 shows the parameters in Equation (1) that are related to the surface geometry. Additional inputs that will aid in the interpretation of β come from tasks conducted in primary

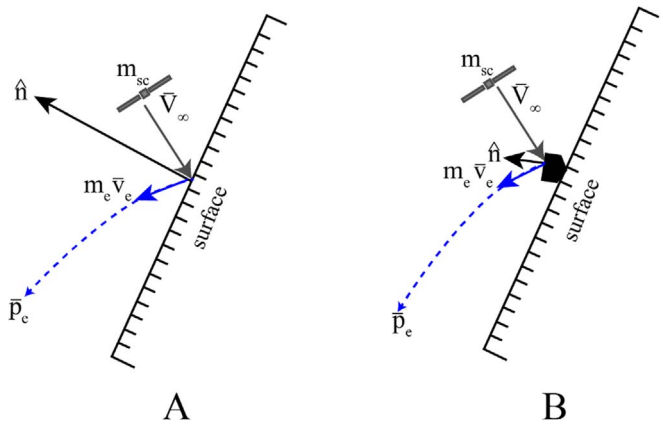

Figure 9. Important parameters in Equation (1), which defines β, are shown here. Panel (a) shows an impact into a smooth surface with incoming spacecraft and outgoing ejecta. The ejecta momentum vector is denoted by $\bar{p}_e$. Panel (b) shows the same vectors with an impact into a block rather than a smooth surface, and a correspondingly different surface normal vector $\bar{p}_n$. None of these vectors are necessarily coplanar save $\boldsymbol{p}_e$ and $\boldsymbol{v}_e$. The vector $\boldsymbol{\epsilon}$ is related to the difference between $\hat{\boldsymbol{n}}$ and $\boldsymbol{v}_e$.

support of the DART-4B requirement and are discussed in Section 6.

6. Requirement DART-4B

The DART-4B Level 1 requirement involves using data from the DART project to characterize the impact site, the ejecta generated by the impact, and the dynamical changes to the Didymos system produced by the DART impact, including a refined determination of β that includes all available observational and physical constraints. The Investigation Team has a number of tasks to support this requirement:

1. *Investigate dynamical effects of the DART impact.* The dynamics models developed to understand the Didymos binary system for DART-1 and DART-2 will be applied to analyze and interpret the dynamical effects of the DART impact, with updates to initial conditions and the shape model derived from DRACO and LICIACube imagery.
2. *Model ejecta from the DART impact through small and large spatial scales.* Observations of the ejecta from the DART impact will be made by LICIACube and attempted by Earth-based and space-based telescopes. Modeling of ejecta on scales relevant both to the

short-term and close-in ("near-field") LICIACube imagery and to longer-term and larger-scale ("far-field") astronomical images has been and continues to be developed to interpret those ejecta observations, to estimate the mass of ejecta and its velocity distribution, and especially to refine the determination of the ejecta momentum direction. Understanding the distribution and amount of the ejecta may provide insights into the dynamical effects of the impact, the target properties, and the dynamical evolution and fate of the ejecta.

3. *Determine and characterize the impact site, refine Dimorphos shape, determine Didymos properties, and image the impact results.* The impact-site location and local characteristics of the impact site will primarily be determined from the analysis of DRACO images, with LICIACube images also used as appropriate. LICIACube will image the results of the impact, constraining the ejecta and possibly the impact crater.
4. *Determine β from the full DART data set and model the ejecta mass and crater size.* The impact models described to support DART-4A will also be applied to model the ejecta mass and crater size resulting from the DART impact. Additional inputs from all DART tasks, as described above, will also be used to produce a refined determination of β and to aid interpretation of the β results for potential future planetary defense applications.

6.1. Investigate Dynamical Effects

Dynamical modeling of the Didymos system informed by available observations (Section 3.1) indicates that there is sensitivity to unknown pre-impact details such as the precise orientation of the primary at a given time (Agrusa et al. 2020). This uncertainty precludes knowing the exact dynamical state of the system prior to impact, although it is assumed that the system will be in or near a relaxed configuration—meaning a near-circular orbit with the secondary long axis nearly aligned with the orbit radial vector and nearly in the equatorial plane of the primary. The impact will excite modes relative to this relaxed state that may be either measurable or inferable based on improved knowledge of the system provided by DRACO and LICIACube (and later Hera). Notably, the difference between the new orbit and spin periods combined with the excited radial oscillations will result in libration of the secondary long-axis orientation around the orbit radial vector in proportion to β (Agrusa et al. 2021). It is possible that the libration could be detectable in light-curve and radar data (Naidu & Margot 2015; Pravec et al. 2016), but it should be readily measurable by Hera, along with a lower limit on the damping timescale. We note that the libration amplitude is also sensitive to the currently poorly constrained shape of the secondary. The orbital radial oscillations will range between 1% and 8% of the mean body separation—for β between 1 and 5, respectively—and corresponding out-of-plane oscillations in the orbit will increase the orbital inclination by between $0\overset{\circ}{.}1$ and $0\overset{\circ}{.}5$, but these motions will not likely be measurable prior to Hera. Note that variation in these results is expected for off-nominal impact velocities/masses, or impact circumstances yielded by launch dates later in the launch period.

If ejecta from Dimorphos impact Didymos, causing landslides or shape deformation, there is a small chance that the gravity perturbation on the orbit of Dimorphos driven by this event may be large enough to be observed in light curves by ground-based telescopes. This event would also change Didymos's spin period, which is key information for separating an orbit change due to the reshaping of Didymos from the one directly caused by the DART impact onto Dimorphos. The required 7.3 s measurement precision for the orbit period (requirement DART-3) will also allow measurement of any change of Didymos's spin period to the same precision, which corresponds to the period change expected if Didymos's short axis length changed by $\sim$1 m (Hirabayashi et al. 2019). The photometric measurement uncertainty may be improved to be $<$0.1 s by the end of 2023 April (Pravec & Scheirich 2018). That spin period change would be equivalent to reshaping of $\sim$1 cm along the short axis. We also note that ground-based observations could characterize Didymos's surface modification by comparing the surface albedo and/or color before and after the impact. Such measurements would significantly help assess Didymos's reshaping and Dimorphos's orbital behavior. Using current DRA values (Section 3.1), we estimate that the upper limit of the timescale of surface mass movement on the primary is $\sim$40 minutes. Ejecta moving faster than 1 m s^{-1} will be gone 20 minutes after the DART impact, and most of the remaining ejecta mass will collide with either Didymos or Dimorphos within 17 days (Yu et al. 2017; Section 6.2). This implies that any dynamical effect will be complete within the post-impact observing window of ground-based telescopes, which lasts more than 6 months after the DART impact, into 2023 March.

Both rigid-body and rubble-pile modeling of the Didymos system using the improved shape models and dynamical configuration knowledge obtained just prior to impact will lead to refined estimates of the pre-impact circumstances and, when coupled with the β measurement (DART-4A) and other observables, estimates of the post-impact configuration. A suite of simulation outcomes consistent with observational constraints for plausible ranges of remaining free parameters will be continually updated before and after impact. The goal will be to find the set of dynamical parameters that most closely match the data. This will help constrain remaining free parameters (perhaps secondary mass, porosity, bulk density, etc.) and possibly improve the accuracy or equivalently reduce the uncertainty of the β estimate.

6.2. Model Ejecta

The DART impact is expected to liberate a large amount of surface material from Dimorphos as ejecta. Studies of the ejecta provide the opportunity to make an estimate of β if the ejecta momentum can be measured sufficiently well. LICIACube will have a flyby distance of 55 km, and its imagery, with a best resolution of 1.4 m pixel^{-1} (Dotto et al. 2021), will be used to determine near-field ejecta properties. LICIACube objectives include multiple images at times and phase angles to allow measurement of ejecta, with an emphasis on measuring ejecta moving at $<$5 m s^{-1} (Dotto et al. 2021). The LICIAcube images are designed to follow plume evolution in the first 300 s with both the Liciacube Explorer Imaging for Asteroid (LEIA) and Liciacube Unit Key Explorer (LUKE) cameras. With this sequence the dynamical characteristics and speed distribution within the plume can be retrieved. Given the timing of the LICIACube flyby (currently planned for 165 s after the DART impact; Dotto et al. 2021), opportunities for plume

imagery may be expected both inbound and outbound for LICIACube.

Cheng et al. (2020) developed an ejecta model relevant to the DART impact into Dimorphos and discussed how imagery can be used to extract information about the impact conditions from the ejecta plume, including using measurements of the plume axis and asymmetry to estimate the ejecta momentum direction. Ejecta mass and velocity distributions can be constrained from the plume optical depth profile and evolution, which can then be tied to physical properties like strength and porosity. The Small Carry-on Impactor (SCI) experiment done by the Hayabusa2 team was analyzed using data from the Deployable Camera (DCAM3) in a similar fashion (Wada et al. 2021), and members of the Hayabusa2 team are also part of the international DART team to lend their experience.

Visualizations are being developed to generate simulated LEIA and LUKE imagery, as well as larger-scale imagery more relevant to astronomical observations, from ejecta models like those in Yu et al. (2017; Yu & Michel 2018) and Cheng et al. (2020). These involve translating the time-evolving 3D-spatial number density field into plane-of-sky appearance. At this writing, work is focusing on simple cases using spherical particles and reasonable assumptions for particle SFD and photometric properties. In the near-field, ejecta particles feel the gravitational acceleration from both binary components, positioned and oriented using the modeling of Full Two-Body Problem (F2BP) dynamical evolution of the binary itself, developed for DART-1 and DART-2 and also employed for DART-4A. Particles also feel throughout near field and far field both differential solar gravity acceleration ("solar tides") and solar radiation pressure (including Didymos and Dimorphos shadowing in the near field). Particles are propagated without tracking interparticle collisions or influencing the binary in any way, so they are essentially treated as an ensemble of test particles in the Restricted Full Three-Body Problem (RF3BP).

In order to quickly interpret data, a suite of simulated images for nominal and off-nominal cases will be rendered prior to the DART impact, along with a pipeline for generating those images from input parameters, to allow real images to be compared to the simulated cases and allow those cases that match the data most closely to be used as bases for more detailed modeling. Forward modeling of simulated images to match data returned from LICIACube and astronomical facilities (Section 6.4), with knowledge of the topography and geology near the site of DART's impact (Section 6.3), will allow estimation of particle properties that fit the evolving ejecta plume, which in turn will inform our understanding of Dimorphos's surface properties.

6.3. Determine and Characterize the Impact Site, Refine Dimorphos Shape, Determine Didymos Properties, and Image the Impact Results

The imaging acquired by DRACO (prior to impact) and LICIACube (both before and after impact) will enhance understanding of the DART impact and its consequences on momentum transfer. The data collected by DART will be used by the Proximity Working Group to address several objectives:

1. *Identify the impact location.* The location of the impact site and its relation to the center of figure of Dimorphos will be determined via the Dimorphos shape modeling effort supporting DART-4A. Current estimates suggest that the impact point will be known relative to the center of figure observed by the DRACO images to <50 cm; radial errors from the center of Dimorphos parallel to the DART velocity vector will be larger (<3.8 m). LICIACube images, which provide stereo parallax data, reduce the radial error; ongoing efforts are characterizing the magnitude of this error reduction.
2. *Assess the target properties.* DRACO images will be used to assess the local target conditions at the impact site. Particular attention will be paid to whether the DART spacecraft impacted a block or regolith, and if any large blocks or other topography nearby may have influenced the excavation of debris from the impact. Impact simulations (Barnouin-Jha et al. 2003; Syal et al. 2016; Susorney et al. 2017) and experiments (Güttler et al. 2012; Tatsumi & Sugita 2018; Barnouin et al. 2019b), including those in situ at Ryugu (Arakawa et al. 2020; Wada et al. 2021), have shown that surface properties can have a substantial effect on the excavation process and resulting momentum transfer. LICIACube has color imaging capability via its LUKE camera, which can provide evidence of or upper limits to color variations across the surface of Dimorphos and between Dimorphos and Didymos at resolutions as fine as 4.3 m pixel^{-1} in the nominal flyby case (Dotto et al. 2021). These data in turn provide insight into the homogeneity of these objects in terms of their composition and/or level of space weathering.
3. *Characterize the impact crater.* LICIACube will attempt to image the DART impact location. If ejecta do not obscure the surface, the images will be used to characterize the DART impact crater. The Proximity Imaging Working Group will analyze the LICIACube images and, by comparison to pre-impact DRACO images, will determine some of the characteristics of the crater, including diameter, depth, and shape, with the caveat that the crater may not have completed forming when it is still resolvable by the LICIACube cameras. Evidence from the Haybusa2 Small Carry-On Impactor (SCI) experiment at Ryugu (Arakawa et al. 2020) and the Touch-And-Go event at Bennu indicates that near-cohesionless surface conditions may be possible on rubble-pile asteroids, and as a consequence very long-lived crater excavation in the weak-gravity regime may occur on Dimorphos.
4. *Characterize the ejecta.* LICIACube will image the DART impact and provide constraints on the resulting ejecta, including the ejecta plume angle, and debris distribution.
5. *Refine the Didymos system properties.* DRACO approach images, including light curves collected when the system is not yet resolved, will enable improved determination of Didymos system properties, such as the rotation rate and orbit of Dimorphos, as well as any updates to the Earth-based, light-curve-derived shape model. The observation geometry from DART and LICIACube on approach is different from what is easily achieved from Earth. The approach images will also help to inform dynamical modeling of the Didymos system and to understand the consequences of the DART impact.

6.4. Constrain the Dynamical Evolution of Ejecta from Telescopic Observations

A series of observations specifically designed to image the impact ejecta will be performed during and following the DART impact. Our primary observing mode to measure the orbit of Dimorphos uses visible-wavelength light with strict requirements on time resolution and observational uncertainty. Our ejecta observations will use longer integration times at a variety of ground- and space-based observatories with a range of wavelengths.

At the time of impact, the focus of our observing program will be to detect the ejecta. We will obtain infrared images from NASA's James Webb Space Telescope (JWST) with time allocated through the Guaranteed Time Observations program. While Didymos's rate of motion exceeds the tracking limit of JWST (108″ per hour) at the time of the DART impact, it drops below that limit on 2022 November 6, and observations will be made on or after that date. In addition, observations are still possible during the period in which it is moving faster than the limit, with the strategy of using the fastest tracking rate available, allowing Didymos to move across the chip. This strategy will be used for observations at the time of the impact itself. Our ability to use ground-based observatories at the time of impact depends on the time selected for impact and the location of the Didymos system relative to Earth at that time. Didymos will be in the southern hemisphere sky, and there are several locations in the southern hemisphere where a lack of telescope facilities could limit our ability to observe the impact itself. DART will support observations from Las Campanas Observatory in Chile and from Las Cumbres Observatory sites in South Africa, Australia, and/or Chile. At this writing, team members have access to additional Southern Hemisphere telescopes in Chile, South Africa, and New Zealand.

Following impact, we will obtain more observations to enable the study of the evolution of the ejecta. We will use the telescopes and observers involved in our light-curve study (DART-3) to obtain periodic images of the system. As the models indicate a growing ejecta plume and corresponding decrease in density, we expect to need longer exposure times to successfully obtain images of the ejecta. We will perform follow-up ground-based observations until the ejecta is no longer visible to our telescopes. We expect the supported observations to be made in commonly used visible-wavelength filters, since these will be used in the light-curve studies. Additionally, we are scheduled to obtain additional JWST infrared images in 2022 November. The JWST measurements at the time of impact will be made using the F164N (1.64 μm) and F323N (3.23 μm) filters, while later characterization will be done via images in those filters and spectroscopically with NIRSpec (0.6–5.3 μm) and MIRI (5–28 μm). If there is abundant ejecta in the decimeter size range, it may be detectable with radar, but that is not thought to be likely.

6.5. Determine β from the Full DART Data Set and Model the Ejecta Mass and Crater Size

Little is known about the shape and material properties of Dimorphos. While initial radar observations (Naidu et al. 2020a) provide an estimate of the moonlet's size, no other resolved images or observations are available. Thus, material properties and structure must be estimated from what is known about meteorites or from other asteroids that have been visited by spacecraft. This provides additional complications to interpreting the impact simulations because a given velocity change may not arise from only one set of unique parameters. The impact simulations described in Section 5.3 cover a wide range of parameter space to reduce this uncertainty. Additional observations (e.g., shape, texture, topography, crater size, color from LICIACube) can help mitigate these uncertainties even more. Thus, additional information that may be available from, for example, LICIAcube and the Proximity Working Group (Section 6.3) and the Observations Working Group (Section 6.4) will be used if available to further refine estimates of β, ejecta mass, and predictions of the crater size.

1. *Using results from proximity imaging.* Information provided by the Proximity Working Group (Section 6.3) can help constrain and refine the inputs to the impact simulations of the DART impact. Images of the impact location allow determination of the local geology (e.g., presence or absence of boulders and whether or not DART hit one), surface tilt, and surface normal ($\hat{\boldsymbol{n}}$). These observations provide important setup parameters to the impact models to ensure that the components of Equation (1) and ϵ are estimated as robustly as possible. Further, while the velocity change imparted by the DART impact, as a singular measurement, will not uniquely determine material parameters such as strength or porosity, information about the ejecta cone properties and the crater size and shape, if available, can provide additional constraints (e.g., Raducan et al. 2019, 2020; Rainey et al. 2020). Information about the ejection angle and thickness of ejecta curtain, as well as how the ejecta curtain evolves in time, from LICIAcube can be used to provide information about the nature of Dimorphos's surface (Richardson et al. 2007; Schultz et al. 2007; Cheng et al. 2020). The potential availability of images of the size and morphology of the DART impact crater from LICIAcube could be used to provide additional constraints on material strength and porosity, as well as potential target structure (e.g., Raducan et al. 2020), as was done for Ryugu from images of the crater caused by their Small Carry-on Impactor (Arakawa et al. 2020; Wada et al. 2021).
2. *Change in rotational period of Didymos.* The Didymos system light curve, determined by the Observations Working Group, is a combination of the rotation period of Didymos and the orbital motion of Dimorphos; therefore, the rotation period of Didymos will be measured as a by-product of determining the orbital period of Dimorphos. Models suggest that there is a very low but nonzero probability that ejecta from the DART impact striking Didymos could cause large-scale mass movement on the primary, resulting in a reshaping of Didymos and a change in its rotation period (Hirabayashi et al. 2019, Section 6.1). Because Dimorphos is so close to Didymos, such an event could potentially produce a change in Dimorphos's orbital period, and that change could be erroneously interpreted as being due to the direct momentum transfer from the DART impact. A determination of whether there is any change in Didymos's rotation period will allow an evaluation of whether this low-probability event has occurred. A preliminary determination of any change in the rotational period of Didymos will be available roughly a month after impact, and if a change is detected, the Dynamics Working Group

would use the dynamical models discussed for DART-1 and DART-2 to assess the change in the orbital period of Dimorphos that was due to the change in Didymos versus that produced by the DART impact.

3. *Measurement of libration of Dimorphos.* Agrusa et al. (2020) showed that the impact of DART into Dimorphos will induce free and forced librations. The amplitudes of these librations are shape dependent, and while calculations of their observability are still being made, it is expected that they will require light-curve precisions better than 0.5% in the most optimistic cases. Measurements of these librations would provide insight into the mass distribution of Dimorphos, but they are unlikely to be measured prior to the arrival of the Hera spacecraft or before the formal completion of the DART project. However, in the event that they are detected by the 2022–2023 telescopic observations, they would allow the assumption of a homogeneous mass distribution to be tested and/or corrected for Dimorphos.

7. Summary

DART, NASA's first planetary defense test mission, must meet four level 1 requirements for mission success. In order to meet these requirements, a series of investigations have been developed, which together will aid in targeting Dimorphos at a time to create the largest deflection, measure the results of that deflection in terms of the period change that is caused, and interpret the DART impact results in terms of its implications for asteroid deflections using the kinetic impact technique.

Just as DART is a test of the kinetic impactor technique, so is the investigation plan a test of what can be inferred from impact and dynamical simulations, Earth-based observations, and spacecraft imagery. The lessons learned from the DART mission, along with the additional data provided by LICIACube and, later, by the Hera mission, will provide key insights into future planetary defense initiatives. Such information will be an invaluable starting point as knowledge of potentially hazardous objects and potential impact mitigation techniques develop over time.

This work was supported in part by the DART mission, NASA Contract No. NNN06AA01C to JHU/APL. A portion of this work was carried out at the Jet Propulsion Laboratory, California Institute of Technology, under a contract with the National Aeronautics and Space Administration (80NM0018D0004). The LICIACube team acknowledges financial support from Agenzia Spaziale Italiana (ASI contract No. 2019-31-HH.0 CUP F84I190012600). P.M. acknowledges funding support from CNES and the European Union's Horizon 2020 research and innovation program under grant agreement No. 870377 (project NEO-MAPP). The work by P.P. and P.S. was supported by the Grant Agency of the Czech Republic, grant 20-04431S. Thanks to the reviewers of this manuscript, both the one who remained anonymous and the one who became Paul Abell. Thanks to JÃ Grier for helping the lead author navigate a pandemic and making some excellent suggestions concerning manuscript issues. We acknowledge the wider contributions of the DART Investigation Team as a whole to the DART Project both up to this point and looking forward. We particularly thank the DART mission systems engineer, Dr. Elena Adams, and all of the team's engineers, who have worked diligently through a pandemic in order to bring DART to the launch pad.

Appendix A
Design Reference Asteroid information

Scope. This appendix captures the reference model of the asteroid 65803 Didymos (provisional name 1996 GT)[14] prior to the 2020–2021 apparition, as of 2021 May 26 (ver. 3.03). It is included here for reference purposes in tabular form as Tables A1–A6.

Terminology and acronyms. The symbol ± refers to the uncertainty of the reported value without giving the nature of the uncertainty. If not stated otherwise, error bars represent 1σ bounds. D is the mean (volume-equivalent) diameter, i.e., the diameter of a sphere with the same volume. Subscripts P, S, and *orb* are for primary, secondary, and orbit of secondary around primary. a_x, b_x, and c_x are the full lengths of the long, intermediate, and short axes of the ellipsoid representing body x.

Measured values are included in bold type to provide a means of rapid identification while scanning the document. They are also noted as "Measured" in the "Measured or Derived from" column.

"Reserved" entries will allow important parameters that are absent from this document to be added later in an appropriate section while maintaining sequential numbering.

Table A1
Permanently Fixed Parameters

Permanently Fixed Parameter	Value	Reference/Comments
Official minor planet number of primary	65803	Minor Planet Center (2004)
Official name of primary	Didymos	Minor Planet Center (2004)
Provisional designation of primary	1996 GT	Minor Planet Center (2004)
Official name of secondary	Dimorphos	Minor Planet Center (2020)

Table A2
Data Sets

Data Set	Affected Parameters	Reference/Comments
Astrometric measurements	10–15	JPL Small Bodies Database Browser
Photometric measurements	1, 2, 21, 22, 23, 25, 26, 30–36	Pravec et al. (2006), Scheirich & Pravec (2009)
Radar measurements	3, 4, 20, 22, 23, 25	Neese et al. (2012), Naidu et al. (2020a)
Spectroscopic measurements	5, 6	De Léon et al. (2006), Dunn et al. (2013)

[14] JPL Small-Body Database Browser entry for Didymos: https://ssd.jpl.nasa.gov/sbdb.cgi?sstr=Didymos.

Table A3
Photometric and Spectroscopic Values

Par #	Parameter	Value	Reference/Comments	Measured or Derived From	Used to Derive
1	Mean absolute magnitude (whole system) *H*	**18.16 ± 0.04**	Pravec et al. (2012)	Measured	3
2	Slope parameter *G*	**0.20 ± 0.02**	Kitazato et al. (2004)	Measured	3
3	Geometric albedo	0.15 ± 0.04	Naidu et al. (2020a)	1, 2, 20, 21	6
4	Radar polarization ratio	**0.20 ± 0.02**	Same sense/opposite sense radar return Neese et al. (2012)	Measured	
5	Spectral type of Didymos	**S-class best fit**	Bus-Demeo classification widget:http://smass.mit.edu/busdemeoclass.html, using spectrum from De Léon et al. (2006)	Measured	6
6	Best meteorite analog	L/LL Chondrite	Dunn et al. (2013)	3, 5	
7	*S*-band, *X*-band radar albedos	**0.20 ± 0.05, 0.30 ± 0.08**	Naidu et al. (2020a)	Measured	
8–9	*Reserved*				

Table A4
Heliocentric Orbit Values

Par #	Parameter	Value	Reference/Comments	Measured or Derived From	Used to Derive
10	Osculating heliocentric eccentricity e	**0.384**	JPL Small Bodies Database Browser	Measured	
11	Osculating heliocentric semimajor axis a	**1.644**	JPL Small Bodies Database Browser	Measured	
12	Osculating heliocentric inclination to the ecliptic i	**3.408 degrees**	JPL Small Bodies Database Browser	Measured	
13	Longitude of the ascending node Ω	**73.199 degrees**	JPL Small Bodies Database Browser	Measured	
14	Argument of perihelion ω	**319°319**	JPL Small Bodies Database Browser	Measured	
15	Time of perihelion passage	**2020 Sep 11.642**	JPL Small Bodies Database Browser	Measured	
16–19	*Reserved*				

Note. These values are provided for those who only require low-precision values. Solution date for Parameters 10–15: 2021 Feb 13 14:47:32.

Table A5
Physical Properties of System and Components

Par #	Parameter	Value	Reference/Comments	Measured or Derived From	Used to Derive
20	Diameter of primary D_P[a]	**780 m ± 30 m**	Naidu et al. (2020a) radar measurement	Measured	3, 21, 22, 23
21	Diameter of secondary D_S^1	164 m ± 18 m	See D_S/D_P below	20, 32	3
22	Bulk density of the primary ρ_P	2170 kg m^{-3} ± 350 kg m^{-3}	Naidu et al. (2020a), from D_P. $M_{\rm tot}$	20, 26, 33	
23	Bulk density of the secondary ρ_S[b]	2170 kg m^{-3} ± 350 kg m^{-3}	See footnote, uncertainty not Gaussian	Assumed same as 22	
24	Secondary elongation a_S/b_S and b_S/c_S[c]	1.3 ± 0.2, 1.2	Based on values from other binary systems; a, b, and c are the full extent of the long, intermediate, and short axes, respectively (Pravec et al. 2016)	Assumed	
25	Distance between the center of primary and secondary a_{orb}	1.20 km ±0.03 km	Naidu et al. (2020a)	26, 33	
26	Total mass of system M	5.55×10^{11} kg $\pm 0.42 \times 10^{11}$ kg.	Naidu et al. (2020a), mass based on Keplerian orbit; does not include shape perturbations	33	25, 23
27	Didymos extents along principal axes x; y; z	**832 ± 25 m; 837 ± 25 m; 786 ± 25 m;**	Reoriented from Naidu et al. (2020a) to be along principal axes; radar measurement of Didymos	Measured	
28–29	*Reserved*				

Notes.
[a] The values of the primary and secondary diameters, as well as the optical and radar albedos, correspond to the baseline pole solution indicated in Section 6. The reported values are volume-equivalent diameters.
[b] The bulk density of the secondary is not known. However, based on the known bulk density range for S-type objects (about 2000–2700 kg m^{-3}), we assume a value of 2170 kg m^{-3} for the secondary to be identical to the primary.
[c] a_S/b_S from P. Pravec et al. (2021, in preparation). Note that we do not have any direct observation of Dimorphos shape. This value is thus assumed from the average value observed for other binary systems. An ellipsoidal shape is assumed with $a_S \geqslant b_S \geqslant c_S$. The assumed b_S/c_S is based on the observations of similar systems. The rotation state is not constrained by observations and may be unstable (tumbling) for $a_S/b_S \sim 1.4$. a_S is oriented along the x-axis of the corotating frame, i.e., in the direction connecting the centers of mass of the two bodies.

Table A6
Pre-impact Binary Orbit Values[a]

Par #	Binary Orbit Solution	Baseline Solution	Reference/Comments	Measured or Derived From	Used to Derive
30	Pole solution	$\lambda = 320°$, $\beta = -79°$ (ecliptic coordinates)	Naidu et al. (2021)	Measured, uses radar shape model and lightcurves	31
31	Obliquity to the heliocentric orbit	$165° \pm 2.2°$	3σ error bars	30	
32	Diameter ratio D_S/D_P[b]	**0.21 ± 0.01**	Scheirich & Pravec (2009)	Measured	21
33	Secondary orbital period P_{orb}	**11.9216287 ± 0.0000031 h (epoch JD 2 452 964.392 15)**	data from 2003–2021.	Measured	40
34	Secondary orbital eccentricity e_{orb}	<0.03	Scheirich & Pravec (2009)	Measured	
35	Rotation period of the primary P_P	**2.260 0 h ± 0.0001 h**	Pravec et al. (2006)	Measured	
36	Rotation period of the secondary P_S	(same as P_{orb})	Assumed in synchronous rotation, to be tested with further observations, Naidu et al. (2020a)	Assumed	
37	Secondary orbital inclination i_{orb} (assumed)	0°	From Naidu et al. (2020b)	Assumed	
38	Obliquity of the primary principal axis with respect to the mutual orbital plane	0°	Assumed, may be updated with further observations	Assumed	
39	Obliquity of the secondary principal axis with respect to the mutual orbital plane (assumed)	0°		Assumed	
40	Mean longitude drift of Dimorphos relative to Keplerian orbit due to BYORP: allowed solutions	$+0.14 \pm 0.1$ °/yr^2	2003–2021 data; 3σ uncertainties.	33	
41	Longitude of ascending node Ω	40°	Naidu et al. (2021), epoch 2011-08-21.5	Assumed. Circular orbit assumption allows parameter to be neglected.	
42	Argument of periapsis ω	Unknown	Will be determined in later apparitions		
43	Mean anomaly M_0	$78.9° \pm 1.9°$	Naidu et al. (2021), epoch 2011-08-21.5	Fits to 2003–2019 data for BYORP = 0.1 solution	

Notes.
[a] Semimajor axis of the binary orbit is included as parameter 25.
[b] Derived from depth of mutual events, so it is a cross-sectional-area-equivalent diameter ratio.

Appendix B
DART's Determination of β: Mathematical Framework

A requirement for DART is to measure the momentum transfer enhancement parameter (β), which is a measure of how much additional momentum beyond that carried by the spacecraft is transferred to the asteroid in a kinetic impact. In a perfectly inelastic collision, with zero net ejecta momentum, $\beta = 1$ by definition. More generally, ejecta caused by the spacecraft impact carry off momentum, effectively giving an extra push and making $\beta > 1$ for the impact.

This appendix presents the definition of β used by the DART project, describes the geometry of the kinetic impact and momentum transfer, and presents the equations and the technical approach to estimate β, first in the classical formulation and then applied to the context of the DART mission. This approach adopts the well-justified approximation that the duration of the impact event is much shorter than the orbital period of Dimorphos and thus happens effectively instantaneously. The result is a "recipe" for estimating β from the data, with a straightforward separation of parameters that are measured, those that are determined via simulations, and those that are assumed.

Background: The parameter β is simply a scale factor, and hence by definition a scalar. However, the vector nature of the overall situation necessitates care. In particular, the ejecta momentum vector, the DART spacecraft momentum vector, and the surface normal vector are not generally collinear, nor even coplanar. One could develop a tensor representation of the ejecta enhancement that would be loosely analogous to β, but that would not advance the objective of generalizing the results of the DART impact experiment to other impact circumstances. Rather, β is a generic parameter intended to afford a prediction of the response of an asteroid in the idealized situation where the asteroid surface is smooth, the surface material is homogeneous, and the impact velocity is along the surface normal vector. Thus, as a part of this formalism, much of the development for computing β is done in components along the surface normal direction at the impact location. Impact circumstances far from this idealized situation would necessarily compromise the utility of any β estimate, just as they would compromise the usefulness of β as a predictive tool in far-from-ideal deflection problems. However, if the surface is not too rough or inhomogeneous (at the appropriate length scale) and the impact is not too oblique, then β remains a valuable means of understanding and modeling an asteroid's response to an impact in general.

This appendix includes the development of the DART estimate of β as derived primarily from the measured change in orbital period, and the inferred change in orbital velocity, at the time of the impact, though many other sources of information do come into play, as detailed below, and will be used in generating the final estimate of β and its associated uncertainty.

The Classical Definition of β: Here we lay out the basic equations and definitions used to compute β in general. See Figure 9 for the geometry of the surface-related parameters. The spacecraft, having mass m_{sc} and relative velocity $\boldsymbol{V}_\infty$ at infinity, impacts a target of mass M at a point at which the outward-pointing surface normal unit vector is $\hat{\boldsymbol{n}}$. The unbound ejecta, having mass m_e and momentum $\boldsymbol{p}_e$ at infinity, emerges at a mass-weighted mean velocity $\boldsymbol{V}_e = \boldsymbol{p}_e/m_e$. Neither the spacecraft velocity $\boldsymbol{V}_\infty$ nor the ejecta velocity $\boldsymbol{V}_e$ is assumed to be in the direction of the unit normal $\hat{\boldsymbol{n}}$, and these three vectors are not necessarily coplanar. The impact results in a velocity change to the target $\Delta\boldsymbol{V}$.

In this framework, the fundamental momentum balance equation for the impact is

$$M\Delta\boldsymbol{V} = m_{sc}\boldsymbol{V}_\infty - m_e\boldsymbol{V}_e. \tag{2}$$

Here the "minus" sign is present because the ejecta momentum is removed from the asteroid momentum, while the spacecraft momentum is added. However, because the ejecta direction is roughly opposite to $\boldsymbol{V}_\infty$, both the spacecraft and ejecta momenta work to increase the magnitude of $\Delta\boldsymbol{V}$.

As detailed below, β is defined in terms of the velocity components along the surface normal vector, which we denote by $V_{e_n} \equiv \boldsymbol{V}_e \bullet \hat{\boldsymbol{n}}$ and $V_{\infty_n} \equiv \boldsymbol{V}_\infty \bullet \hat{\boldsymbol{n}}$. (Note that $V_{\infty_n} < 0$ because the spacecraft velocity $\boldsymbol{V}_\infty$ is roughly opposite to the surface normal $\hat{\boldsymbol{n}}$.) We also need the components of the spacecraft and ejecta velocity that are orthogonal to the surface normal. For the spacecraft velocity we have

$$\boldsymbol{V}_{\infty_{\perp n}} \equiv \boldsymbol{V}_\infty - V_{\infty_n}\hat{\boldsymbol{n}},$$

and for the ejecta velocity we have

$$\boldsymbol{V}_e = (\hat{\boldsymbol{n}} + \boldsymbol{\epsilon})V_{e_n}.$$

The small vector $\boldsymbol{\epsilon}$ is perpendicular to $\hat{\boldsymbol{n}}$ and has a magnitude equal to tan α, where α is the angle between the ejecta momentum and the normal.

Now we can introduce the classical definition of β, which is defined as the ratio between the total momentum change $M\Delta\boldsymbol{V}$ and the input momentum $m_{sc}\boldsymbol{V}_\infty$, *in projection onto the surface normal direction*. Thus, by definition

$$\beta = \frac{m_{sc}V_{\infty_n} - m_eV_{e_n}}{m_{sc}V_{\infty_n}},$$

and so we have

$$m_eV_{e_n} = -(\beta - 1)m_{sc}V_{\infty_n},$$

recalling that $V_{\infty_n} < 0$. This is consistent with the definition used, for example, by Feldhacker et al. (2017). With these definitions, the momentum balance equation (Equation (1)) can now be written in components along and across the surface normal

$$\Delta\boldsymbol{V} = \frac{m_{sc}}{M}[\beta V_{\infty_n}\hat{\boldsymbol{n}} + \boldsymbol{V}_{\infty_{\perp n}} + (\beta - 1)V_{\infty_n}\boldsymbol{\epsilon}]. \tag{3}$$

Note that this is a complete formulation that does not assume that the spacecraft or ejecta momenta are aligned with the surface normal vector. However, the utility of the formulation in terms of β still depends on the assumptions outlined above. In the idealized case, where both the impact and ejecta velocities are along the surface normal vector, the equation simplifies to the more usual form

$$\Delta\boldsymbol{V} = \frac{m_{sc}}{\mathrm{M}}\beta V_{\infty_n}\hat{\boldsymbol{n}}.$$

Application to DART: the DART mission will detect the impact-induced change in orbital velocity by virtue of a change in orbital period P. The period change ΔP is directly measured through ground-based observations of the timing of mutual events and is reflective of the change in the magnitude of the orbital velocity. Equivalently, we can say that ΔP determines the along-track component $\Delta V_T = \Delta\boldsymbol{V} \bullet \hat{\boldsymbol{e}}_T$ of the impact-induced change in velocity. Here we use the unit vector of

Table B1
Source of Data Inputs to the DART Estimate of β

Parameter	Definition—Source
ΔP	Change in orbital period of satellite due to DART impact—derived from timing of ground-based mutual event observations
ΔV_T	Along-track change in orbital velocity—obtained from ΔP and the binary mutual orbit parameters
m_{sc}	Spacecraft mass—estimated from fuel consumption and known dry mass value
$\hat{\boldsymbol{e}}_T$	Unit vector describing satellite orbital velocity at impact—derived from orbit and impact time
$\hat{\boldsymbol{n}}$	Surface normal unit vector at the impact site—shape modeling
$\boldsymbol{V}_\infty$	Impact velocity—spacecraft navigation
V_{∞_n}	Component of impact velocity in normal direction—computed from $V_{\infty_n} = \boldsymbol{V}_\infty \bullet \hat{\boldsymbol{n}}$
$V_{\infty_{\perp n}}$	Component of impact velocity orthogonal to normal direction—computed from $\boldsymbol{V}_{\infty_{\perp n}} = \boldsymbol{V}_\infty - V_{\infty_n}\hat{\boldsymbol{n}}$
M	Target mass—shape and volume from DART and LICIACube imaging, and radar measurements of system, assuming uniform bulk density across Didymos system
$\boldsymbol{\epsilon}$	Offset vector between surface normal direction and ejecta velocity vector—derived from impact simulation and modeling given the known $\boldsymbol{V}_\infty$ and $\hat{\boldsymbol{n}}$.

Note. For clarity, variables in Equation (4) and elsewhere are obtained as described above.

the orbital velocity $\hat{\boldsymbol{e}}_T = \boldsymbol{V}_B/V_B$, where $\boldsymbol{V}_B$ and $V_B = \|\boldsymbol{V}_B\|$ represent the orbital velocity with respect to Didymos at impact.

With ΔV_T derived from mutual events we can now estimate β by projecting the momentum balance equation (Equation (3)) onto the $\hat{\boldsymbol{e}}_T$ direction:

$$\Delta V_T = \Delta \boldsymbol{V} \bullet \hat{\boldsymbol{e}}_T = \frac{m_{sc}}{M} \times [\beta V_{\infty_n}\hat{\boldsymbol{n}} + \boldsymbol{V}_{\infty_{\perp n}} + (\beta - 1)V_{\infty_n}\boldsymbol{\epsilon}] \bullet \hat{\boldsymbol{e}}_T.$$

Solving for β yields

$$\beta = \frac{\frac{M}{m_{sc}}\Delta V_T - \boldsymbol{V}_{\infty_{\perp n}} \bullet \hat{\boldsymbol{e}}_T + V_{\infty_n}\boldsymbol{\epsilon} \bullet \hat{\boldsymbol{e}}_T}{V_{\infty_n}(\hat{\boldsymbol{n}} + \boldsymbol{\epsilon}) \bullet \hat{\boldsymbol{e}}_T}. \quad (4)$$

This equation is an *exact result*, which captures all of the essential physics without unnecessary assumptions. Once β is estimated from this equation, the other (unobserved) components of $\Delta \boldsymbol{V}$, i.e., those in the radial and out-of-plane directions, can be obtained by returning to Equation (3), where all terms on the right-hand side are now known. Importantly, in this formulation β does not depend on the reference frame in which the measurements are taking place, e.g., the orbit frame.

Despite the "classical" definition of β, both the non-normal component of the spacecraft velocity and the non-normal component of the ejecta momentum are involved in getting the correct answer. This is because these non-normal components can contribute to the along-track ΔV_T (if $\hat{\boldsymbol{e}}_T$ and $\hat{\boldsymbol{n}}$ are not the same) and thereby to the period change. The terms involving $\boldsymbol{V}_{\infty_{\perp n}}$ and $\boldsymbol{\epsilon}$ in Equation (4) are needed to "decontaminate" the ΔV_T determination and return a value of β consistent with its definition.

Each of the measured, derived, or simulated quantities on the right-hand side of Equation (4) will be obtained with error bars, or as probability density functions (pdfs). Correctly propagating the errors (convolving the pdf's) will give the uncertainty interval for β.

The formulation in Equation (4) clearly shows the role of each piece of DART data in the process of estimating β. Table B1 consolidates details on how each of the terms in Equation (4) is to be obtained, but we first expand briefly on four key quantities that feed into the β estimate, namely, ΔV_T, M, $\hat{\boldsymbol{n}}$, and $\boldsymbol{\epsilon}$.

Estimate of along-track change in orbital velocity of Dimorphos (ΔV_T): Given the change ΔP in the pre-impact orbital period P, an approximate value for the transverse velocity change ΔV_T can be derived from elementary orbital mechanics according to

$$\Delta V_T = \left(\frac{an}{V_B}\right)^2 \frac{\Delta P}{3P} V_B. \quad (5)$$

Here a is the pre-impact binary system osculating semimajor axis and $n = \frac{2\pi}{P}$ is the mean motion (not to be confused with the surface normal unit vector $\hat{\boldsymbol{n}}$ used elsewhere in this paper). The orbital period P is known from pre-impact mutual event observations, while the change ΔP is obtained from post-impact mutual event observations. The semimajor axis a is derived from radar observations of the Didymos system.

Note that Equation (5) is an approximation, though it does not assume a circular orbit. In the circular case $V_B = an$, and so the quantity in parentheses goes to unity. Equation (5) does, however, make the following assumptions:

1. That the period change is small relative to the orbital period, because for large period changes ΔV_T does not change linearly with $\frac{\Delta P}{P}$. This assumption introduces relative errors in ΔV_T similar to the relative period change $\frac{\Delta P}{P}$. Thus, for DART it introduces errors of $\sim$2%–3% in ΔV_T, assuming $1 < \beta < 2$. Should it be needed, a less compact but fully analytic expression that removes this assumption is readily obtained.
2. That the orbital motion is Keplerian, and thus the effects of nonspherical gravitational fields from both the primary and secondary are neglected. This formulation can readily be extended to include gravitational harmonics, with J_2 for Didymos likely being the most important.
3. That the gravitational field of the primary is unchanged by the DART impact. Should the primary be reshaped

by impacts of DART-driven ejecta on its structurally sensitive surface, the modification of the gravity field can be estimated by ground-based observations of the change in the primary's spin period.

In the actual analysis leading to the DART estimate of β, each of these assumptions will be carefully evaluated and either removed through a more involved formulation or captured in the associated uncertainty analysis.

Estimate of Dimorphos shape ($\boldsymbol{M}$ and $\hat{\boldsymbol{n}}$): DRACO images will provide the main data sets for a shape model for Dimorphos. These data will be augmented by LICIACube imagery, particularly of the "far side" of Dimorphos, which is the side facing away from the inbound imagery. The shape model, along with density estimates based on other asteroid satellites (Table 4), will be used to provide an estimate of the target mass M.

Impact-site imagery from DRACO will allow a detailed characterization of the topography of the impact site in the form of digital terrain maps, which will directly yield the surface normal vector $\hat{\boldsymbol{n}}$ at the impact site. Determining the appropriate length scale for averaging the impact-site topography to derive the normal vector to be used in Equation (4) is an impact simulation task.

Estimate of the non-normal component of ejecta momentum: ($\boldsymbol{\epsilon}$). Impact simulations provide information about the crater formation, including ejecta generation, following the DART impact. The mass and velocity distributions for the ejecta can be calculated for a given simulation, and the ejecta momentum with respect to the surface normal vector can be determined. This leads to a direct estimate of the ejecta offset vector $\boldsymbol{\epsilon}$ for each assumed set of surface parameters. Also, as a part of the impact simulations, the appropriate averaging length scale for computing $\hat{\boldsymbol{n}}$ can be derived. By surveying the space of material physical properties and topographic parameters, the impact simulation experiments will provide crucial guidance in assessing uncertainties, and in particular the effect of extreme topography at the impact site.

In this formulation, hydrodynamic impact simulations are needed only to predict the direction of the ejecta. But this is not a small job, since the prediction needs to take into account the likely ranges of all physical properties of the surface, including porosity, inhomogeneity, and so on. Moreover, the role of simulations does not end with this "first determination of β" that satisfies requirement DART-4a. Any additional data that may be obtained from ground-based telescopes, LICIACube, or Hera—which could include imaging of the ejecta plume, detections of orbital eccentricity or precession, and close-up images of the crater—will need to be folded through simulations to determine what constraints they put on material properties and how these constraints lead to improved estimates for β (requirement DART-4b), as well as understanding other components of the momentum transfer besides the normal one.

ORCID iDs

Andrew S. Rivkin https://orcid.org/0000-0002-9939-9976
Nancy L. Chabot https://orcid.org/0000-0001-8628-3176
Angela M. Stickle https://orcid.org/0000-0002-7602-9120
Cristina A. Thomas https://orcid.org/0000-0003-3091-5757
Derek C. Richardson https://orcid.org/0000-0002-0054-6850
Olivier Barnouin https://orcid.org/0000-0002-3578-7750
Carolyn M. Ernst https://orcid.org/0000-0002-9434-7886
Steven Chesley https://orcid.org/0000-0003-3240-6497
Shantanu Naidu https://orcid.org/0000-0003-4439-7014
Thomas S. Statler https://orcid.org/0000-0003-4909-9542
Brent Barbee https://orcid.org/0000-0003-3739-3242
Harrison Agrusa https://orcid.org/0000-0002-3544-298X
Nicholas Moskovitz https://orcid.org/0000-0001-6765-6336
R. Terik Daly https://orcid.org/0000-0002-1320-2985
Petr Pravec https://orcid.org/0000-0001-8434-9776
Petr Scheirich https://orcid.org/0000-0001-8518-9532
Elisabetta Dotto https://orcid.org/0000-0002-9335-1656
Vincenzo Della Corte https://orcid.org/0000-0001-6461-5803
Patrick Michel https://orcid.org/0000-0002-0884-1993
Michael Küppers https://orcid.org/0000-0002-5666-8582
Justin Atchison https://orcid.org/0000-0002-2121-5209

References

Agrusa, H. F., Derek, C. R., Alex, B. D., et al. 2020, Icar, 113849
Agrusa, H. R., Gkolias, I., Tsiganis, K., et al. 2021, Icar, in press (doi:10.1016/j.icarus.2021.114624)
Arakawa, M., Saiki, T., Wada, K., et al. 2020, Sci, 368, 67
Barnouin, O. S., Daly, M. G., Palmer, E. E., et al. 2020, P&SS, 180, 104764
Barnouin, O. S., Daly, R. T., Cintala, M. J., & Crawford, D. A. 2019a, Icar, 325, 67
Barnouin, O. S., Daly, R. T., Ernst, C. M., Palmer, E. E., & Daly, M. 2019b, LPSC, 52, 2448
Barnouin-Jha, O. S., Cintala, M. J., & Crawford, D. A. 2003, in Third International Conf. on Large Meteorite Impacts (Nördlingen), 4106
Binzel, R. P., Rivkin, A. S., Stuart, J. S., et al. 2004, Icar, 170, 259
Cheng, A. F., Rivkin, A. S., Michel, P., et al. 2018, P&SS, 157, 104
Cheng, A. F., Stickle, A. M., Fahnestock, E. G., et al. 2020, Icar, 352, 113989
Cùk, M., & Burns, J. A. 2005, Icar, 176, 418
Cùk, M., & Nesvorny`, D. 2010, Icar, 207, 732
De Léon, J., Licandro, J., Duffard, R., & Serra-Ricart, M. 2006, AdSpR, 37, 178
Dotto, E., Della Corte, V., Amoroso, M., et al. 2021, P&SS, 199, 105185
Dunn, T. L., Burbine, T. H., Bottke, W. F., Jr, & Clark, J. P. 2013, Icar, 222, 273
Feldhacker, J. D., Bruck Syal, M., Jones, B. A., et al. 2017, JGCD, 40, 2417
Flynn, G. J., Consolmagno, G. J., Brown, P., & Macke, R. J. 2018, ChEG, 78, 269
Gaskell, R. W., Barnouin-Jha, O. S., Daniel, J. S., et al. 2008, M&PS, 43, 1049
Güttler, C., Hirata, N., & Nakamura, A. M. 2012, Icar, 220, 1040
Hirabayashi, M., Davis, A. B., Fahnestock, E. G., et al. 2019, AdSpR, 63, 2515
Holsapple, K. A., & Housen, K. R. 2012, Icar, 221, 875
Jutzi, M., & Michel, P. 2014, Icar, 229, 247
Kitazato, K., Abe, M., Mito, H., et al. 2004, LPSC, 35, 1623
Margot, J.-L., Pravec, P., Taylor, P. A., Carry, B., & Jacobson, S. A. 2015, in Asteroids IV, ed. P. Michel, F. E. DeMeo, & W. F. Bottke, Vol. 1 (Tucson, AZ: Univ. Arizona Press), 355
Michel, P., Kueppers, M., Sierks, H., et al. 2018, AdSpR, 62, 2261
Minor Planet Center 2004, MPC, 52326
Minor Planet Center 2020, MPC, 2020-M83
Moskovitz, N. A. 2012, Icar, 221, 63
Naidu, S., Benner, L., Brozovic, M., et al. 2020a, Icar, 348, 113777
Naidu, S. P., Chesley, S. R., & Farnocchia, D. 2020b, Jet Propulsion Laboratory Interoffice Memorandum 392R-20-001
Naidu, S. P., Chesley, S. R., & Farnocchia, D. 2021, Jet Propulsion Laboratory Interoffice Memorandum 392R-21-004
Naidu, S. P., & Margot, J.-L. 2015, AJ, 149, 80
Naidu, S. P., Margot, J. L., Taylor, P. A., et al. 2015, AJ, 150, 54
Neese, C., Benner, L. A. M., & Ostro, S. J. (ed.) 2012, Asteroid Radar V18.0. EAR-A-5-DDR-RADAR-V18.0. NASA Planetary Data System
Ostro, S. J., Margot, J. L., Benner, L. A., et al. 2006, Sci, 314, 1276
Owen, M., Bruck Syal, M., Graninger, D., Remington, T., & Howley, K. 2019, EPSC-DPS Joint Meeting, 13, 1279
Pravec, P., Fatka, P., Vokrouhlický, D., et al. 2019, Icar, 333, 429
Pravec, P., Harris, A. W., Kušnirák, P., Galád, A., & Hornoch, K. 2012, Icar, 221, 365
Pravec, P., & Scheirich, P. 2018, in 42nd COSPAR Scientific Assembly, S-3

Pravec, P., Scheirich, P., Kušniràk, P., et al. 2006, Icar, 181, 63
Pravec, P., Scheirich, P., Kušnirák, P., et al. 2016, Icar, 267, 267
Raducan, S. D., Davison, T. M., & Collins, G. S. 2020, P&SS, 180, 104756
Raducan, S. D., Davison, T. M., Luther, R., & Collins, G. S. 2019, Icar, 329, 282
Rainey, E. S., Stickle, A. M., Cheng, A. F., et al. 2020, IJIE, 103528
Richardson, J. E., Melosh, H. J., Lisse, C. M., & Carcich, B. 2007, Icar, 191, 176
Scheeres, D. J., McMahon, J. W., Jones, B. A., & Doostan, A. 2015, IEEE Aerospace Conference (Piscataway, NJ: IEEE), 1
Scheirich, P., & Pravec, P. 2009, Icar, 200, 531
Scheirich, P., Pravec, P., Kušnirák, P., et al. 2021, Icar, 360, 114321
Scheirich, P., Pravec, P., Thomas, C. A. & the Didymos Observer Team 2019, EPSC-DPS Joint Meeting, 13, 473
Schultz, P. H., Eberhardy, C. A., Ernst, C. M., et al. 2007, Icar, 191, 84
Stickle, A. M., Atchison, J. A., Barnouin, O. S., et al. 2015, Procedia Engineering, 103, 577
Stickle, A. M., Rainey, E. S. G., Syal, M. B., et al. 2017, Procedia Engineering, 204, 116
Stickle, A. M., Syal, M. B., Cheng, A. F., et al. 2020, Icar, 338, 113446
Susorney, H. C., Barnouin, O. S., Stickle, A. M., et al. 2017, Procedia Engineering, 204, 421
Syal, M. B., Owen, J. M., & Miller, P. L. 2016, Icar, 269, 50
Tatsumi, E., & Sugita, S. 2018, Icar, 300, 227
Viikinkoski, M., Kaasalainen, M., & Ďurech, J. 2015, A&A, 576, A8
Vokrouhlický, D., & Nesvorný, D. 2008, AJ, 136, 280
Wada, K., Ishibashi, K., Kimura, H., et al. 2021, A&A, 647, A43
Walsh, K. J., & Jacobson, S. A. 2015, in Asteroids IV, ed. P. Michel, F. E. DeMeo, & W. F. Bottke (Tucson, AZ: Univ. Arizona Press), 375
Weaver, H. A., Buie, M. W., Buratti, B. J., et al. 2016, Sci, 351, aae0030
Wolters, S. D., Ball, A. J., Wells, N., Saunders, C., & McBride, N. 2011, P&SS, 59, 1506
Wolters, S. D., Weissman, P. R., Christou, A., Duddy, S. R., & Lowry, S. C. 2014, MNRAS, 439, 3085
Yu, Y., & Michel, P. 2018, Icar, 312, 128
Yu, Y., Michel, P., Schwartz, S. R., Naidu, S. P., & Benner, L. A. M. 2017, Icar, 282, 313
Zhang, Y., Derek, C. R., Olivier, S. B., et al. 2017, Icar, 294, 98